THESIS

INVESTIGATING POTENTIAL GROUNDWATER OUTFLOWS:

COTTONWOOD SUB-BASIN, JOSHUA TREE NATIONAL PARK, CALIFORNIA, USA

Submitted by

John Boyle

Department of Geosciences

In partial fulfillment of the requirements

For the Degree of Master of Science

Colorado State University

Fort Collins, Colorado

Summer 2019

Master's Committee:

Advisor: William Sanford

Michael Ronayne
Pinar Omur-Ozbek
Forrest Harvey

ABSTRACT

INVESTIGATING POTENTIAL GROUNDWATER OUTFLOWS: COTTONWOOD SUB-BASIN, JOSHUA TREE NATIONAL PARK, CALIFORNIA USA

This study utilizes Electrical Resistivity Tomography (ERT) to investigate potential groundwater outflows of the Cottonwood sub-basin (CsB) in Joshua Tree National Park (JOTR), California. Southern JOTR depends on one groundwater well (LUB-23) screened in an unconfined aquifer unlike the northern section which obtains its water from the municipal water system of the town of Joshua Tree. Depth to water was reported at 67m (219 ft) below ground surface (bgs) in 2017, a drop of almost 15m (49 ft) since installation in 1958. This variability in water level drives the need for a definitive water budget particularly since there is only one groundwater well. To contribute to developing a water budget, this study focused on investigating a potential groundwater connection between the CsB and the larger neighboring Pinto Basin. Interpretation of the subsurface resistivity models showed lack of a groundwater connection (or lack of contiguous low resistivity distribution) thus, this study concludes there is no groundwater connection or underflow at the boundary of the CsB and the Pinto Basin.

Depth to water readings, which confirmed the water table was at 58m (190 ft) bgs. suggest the reported depth to water of 67m (219 ft) did not likely represent the static water level. Water quality and stable isotope analyses of groundwater samples were collected and compared to analyses performed from 2009 showing little variability over the 9-year period between sampling. Thus, no indications that pumping has modified chemistry or isotope composition.

ACKNOWLEDGEMENTS

This research would not have been possible without the patient mentorship of my advisor Dr. William E. Sanford, who has my genuine appreciation for all his efforts. My understanding of all the topics required for this study grew from an infancy under his direct tutelage and a simple acknowledgement cannot express the depth of impact he has had on me both personally and professionally. I would also like to recognize and thank my committee members Dr. Michael Ronayne, Dr. Pinar Omur-Ozbek, and Dr. Forrest "Ed" Harvey who each contributed greatly to my grasp of the subject matter, related subject matter, or oversaw resourcing going beyond expectations to make themselves available for my development. A special thank you to National Park Service Water Resource Division hydrologist Steven Rice who not only co-authored the original work this study is built on, but mentored me on the geophysical exploration concepts to a point that yielded decisive conclusions. The field work would have been a resounding failure without the group of savants that came together to make it possible: JOTR staff: Allison Dunkel and Luke Sabala, and fellow graduate student Tyler Gilkerson. Never again will I trivialize the impact of hand-carrying hundreds of pounds of equipment through kilometers of wilderness. Thank you all for your selfless contributions.

TABLE OF CONTENTS

LIST OF TABLES

LIST OF FIGURES

1. INTRODUCTION

Within the Joshua Tree National Park (JOTR) in southern California (Figure 1-1), the majority of infrastructure water is provided from the municipal water system from the town of Joshua Tree, CA. Currently, the southern part of the park obtains its water supply from a groundwater well located in the Cottonwood sub-basin of the Pinto Basin. This well has been referred to by many different names, but will herein be referred to as LUB-23 (LUB-23 refers to the Mathany's identification of it as a Low-Use Basin well in the 2012 publication on groundwater quality) (Mathany, et al., 2012). Installed in 1958, LUB-23 provides water for the Cottonwood visitor center, park employee housing, and southern infrastructure for the park such as water treatment and storage (Figure 1-2). Recently, an initiative has developed to expand the Cottonwood visitor center in JOTR in order to accommodate a greater tourism presence. This potential growth drives the need to have an accurate water budget for an area with only one groundwater well.

Previous geophysical studies indicate that local groundwater which supplies LUB-23 is likely contained within a small sub-basin of the larger Pinto Basin, Cottonwood sub-basin, which is 5% the size of the Pinto Basin, at ~8,900 hectares in size compared to ~165,000 hectares (22,000 – 407,000 acres) (Figure 1-3; Karst & Rice, 2018). Overland flow from precipitation in the surrounding mountains concentrates into the Smoke Tree Wash (the primary surface drainage in the area of interest) and percolates into the Cottonwood sub-basin (Figure 1-4). Powell's geologic interpretation (2001) of the Cottonwood sub-basin infers several faults near the boundary of the Cottonwood sub-basin and the Pinto basin. Weir & Bader (1963) suggest that faults could create a localized change in hydraulic gradient which may set conditions for a

groundwater connection across this boundary (Weir & Bader, 1963). A groundwater connection between the basins could serve as an additional outflow previously unidentified, but if it currently exists, it likely has existed since before development.

In 2018, park personnel reported the depth to water in LUB-23 production well at 67m (219 ft) below ground surface (bgs), a drop of approximately 15m (49 ft) over several decades (Karst & Rice, 2018). A water budget analysis performed by Karst and Rice (2018) suggested that groundwater pumping alone would not cause such declines, but does not detail potential underflows from the Cottonwood Basin. Karst and Rice (2018) cited potential causes of water level declines that include underflows via a fault controlled-spillway or LUB-23 becoming inefficient from blocked or clogged screens. Karst and Rice (2018) also proposed a location to place a second groundwater well in the Cottonwood Sub-basin to serve as a contingency well, monitoring well, or primary production well. The well siting recommendation was based on gravity data acquired in 2007 to determine the deepest part of the basin arguing it is the most advantageous location for the second well (Langenheim et al., 2016).

Measured water level declines at LUB-23 may reflect substantial changes in aquifer storage, highlighting the need to better characterize water budget components. This present study investigated the presence of faulting and groundwater connections between the Cottonwood sub-basin and Pinto Valley but not what may have caused the connection.

The overall motivation behind this study is to compliment the research conducted by the National Park Service in 2018 and contribute to a refined hydrogeologic conceptual model. There are two conceptual scenarios that would result in the presence of a groundwater connection between the Cottonwood sub-basin and the Pinto Basin by a fault-controlled spillway. Scenario A is the circumstance where the local water table responds to recharge and, at

some point, the water table rises above a fault boundary to the adjoining basin, and creates a groundwater connection (Figure 1-5). Scenario B is the circumstance where there is a groundwater connection into the Pinto Basin by means of flow through fractures in the basin-bounding fault (Figure 1-5).

Bense et al (2013) highlight the uncertainty in the ability to determine hydrogeology characteristics and influences in fault zone areas. Faults can act as conduits allowing fluid transport and is fundamental to understanding influences on hydrogeological characteristics to include groundwater flow (Sibson, 1981). At shallow depths fluid properties do not influence geologic processes of fault behavior as they do at greater depths as a result of fluid pressure. Therefore, it is easier to predict groundwater behavior from the geologic properties of the fault (Sibson et al., 1975). The primary characteristics of interest would be the hydraulic gradient and the resulting permeability of the fault due to compaction and deformation. Ultimately the fault zone could act as a conduit for groundwater flow or as a barrier to isolate one basin from the other. A conceptual illustration of fault architecture (Figure 1-6) shows how, depending on the degree of deformation, faults can contribute to isolating or acting as a conduit (Bense, et al., 2013). Thus, characterizing a fault zone can prove informative and help understand the hydrogeologic relationships.

Electrical Resistivity Tomography (ERT) was used to investigate the groundwater connections between the basins and to validate the recommendations of a secondary well site by Karst and Rice (2018). ERT was chosen because it is minimally invasive (being minimally invasive is of importance because the study area is in designated federally protected wilderness area), can image to the desired resolution and to the depth estimated for the bedrock surface, and can show groundwater connections in the subsurface.

The use of ERT to investigate faults can be informative as is evidenced in Monahan's investigation of the Los Osos fault zone in southern California, a study area with similar climate, stratigraphy, and fault frequency as JOTR (Monahan, 2013). She found strong lateral contrasts that inferred a dipping fault as well as low resistivity zones that correlated with saturated alluvial deposits. The success of using ERT is in its ability to differentiate between sediment layers and illustrate the orientation of the fault between the hanging wall and the foot wall (Monahan, 2013). Therefore, this study investigating a potential fault-controlled spillway in JOTR will use ERT to try to identify these same characteristics in the survey area.

To contribute to data needed to perform a water budget, the objectives of this study are to: (1) investigate groundwater connections between the Cottonwood sub-basin and the Pinto Basin using ERT, (2) investigate the efficiency of LUB-23, (3) conduct an analysis of water quality at LUB-23, and (4) evaluate the recommendation of a secondary well site by Karst and Rice (2018). Water quality analyses were also conducted through geochemical sampling to show any evidence of groundwater contamination or suggestions that the well is drawing water from new sources compared to 2009 sampling. Using a well sounder and subsurface camera, a well investigation was conducted to identify any potential characteristics that would inhibit the efficient operation of the groundwater pump or screening of LUB-23.

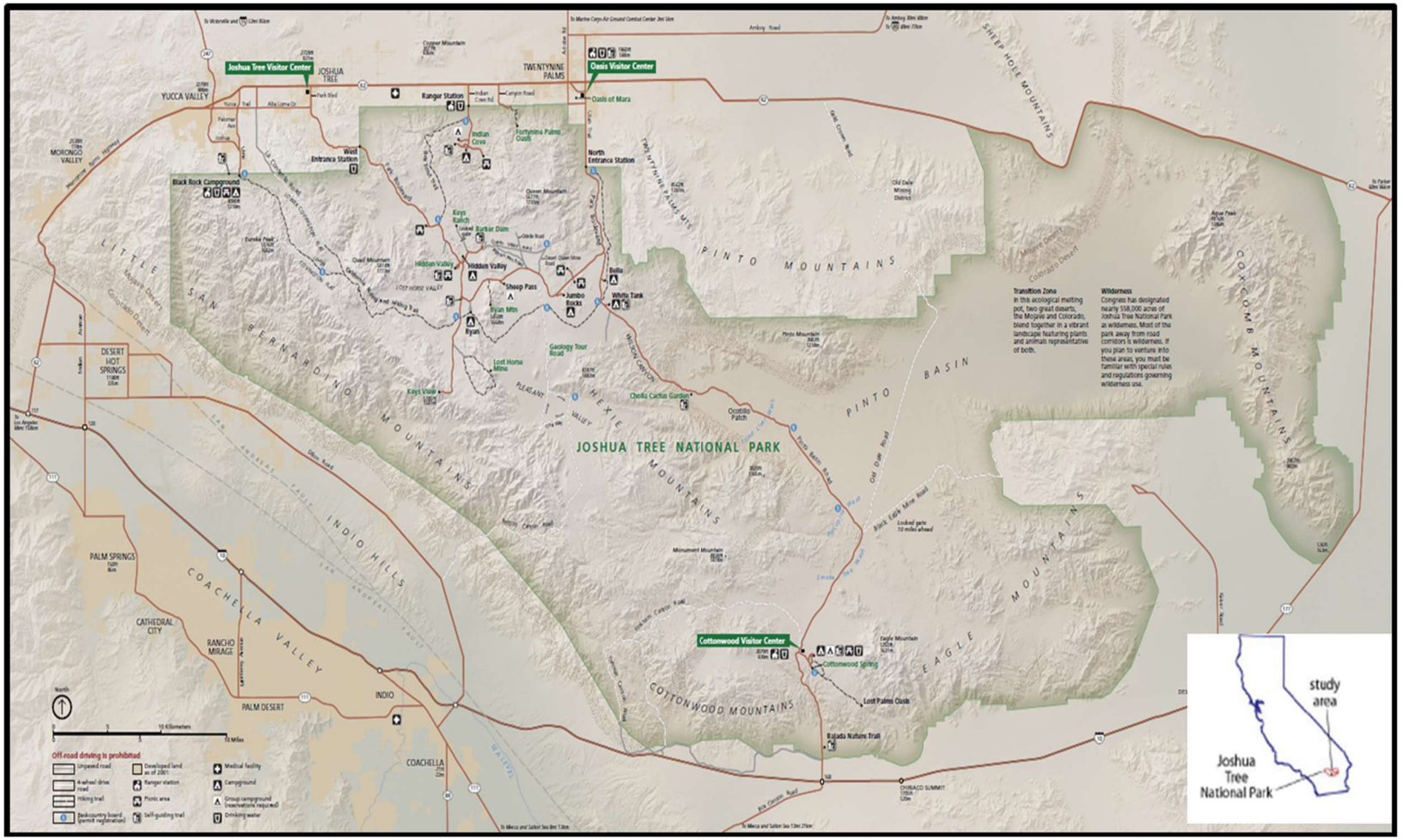

Figure 1-1. Joshua Tree National Park Orientation. Modified from source credit: National Park Service: Joshua Tree National Park (https://www.nps.gov/jotr/planyourvisit/maps.htm)

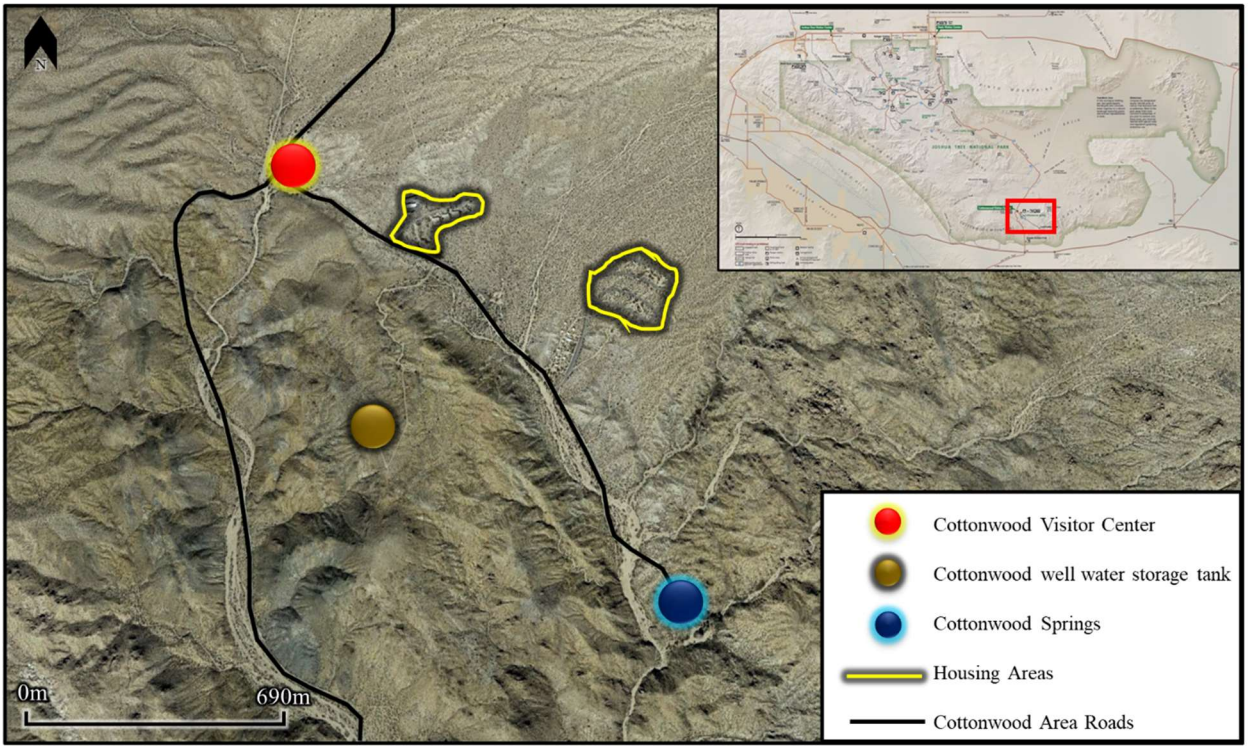

Figure 1-2. Cottonwood Area Infrastructure.

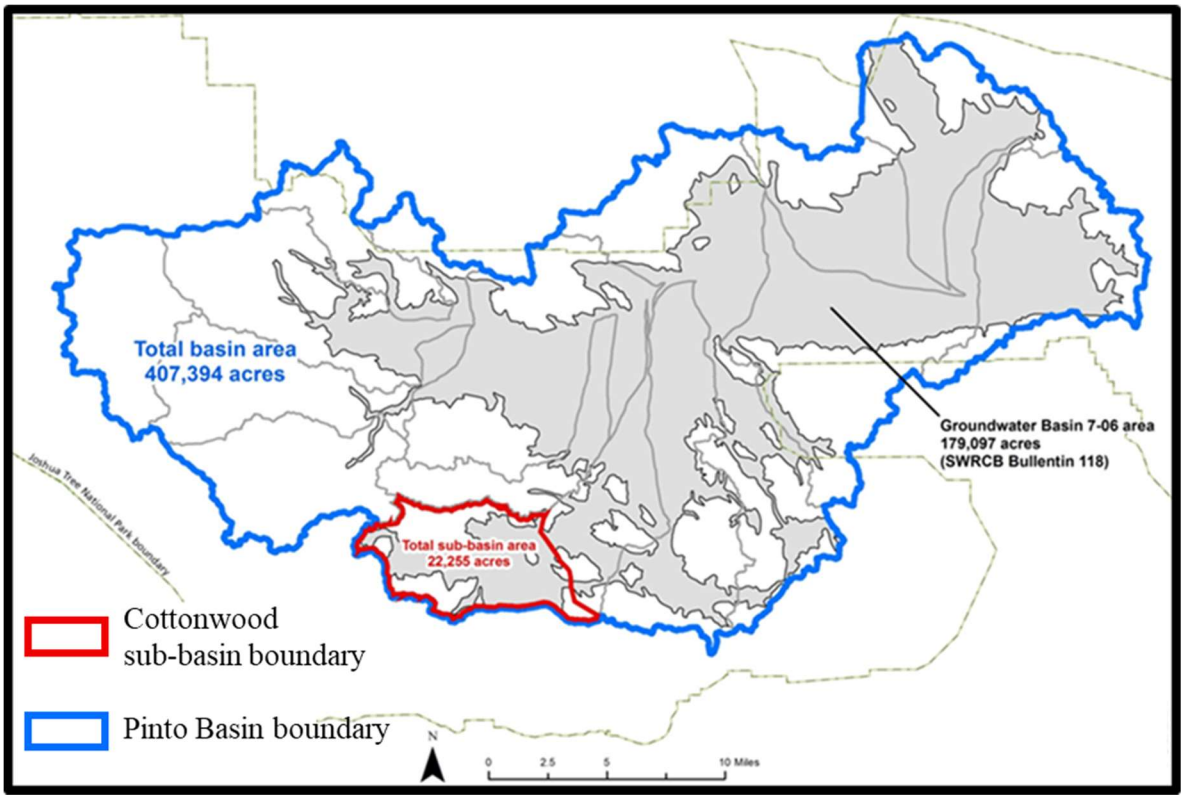

Figure 1-3. Cottonwood Sub-Basin Orientation, Joshua Tree National Park, California. Source credit: National Park Service – Lake Mead National Recreation Area GIS Office, April 2018.

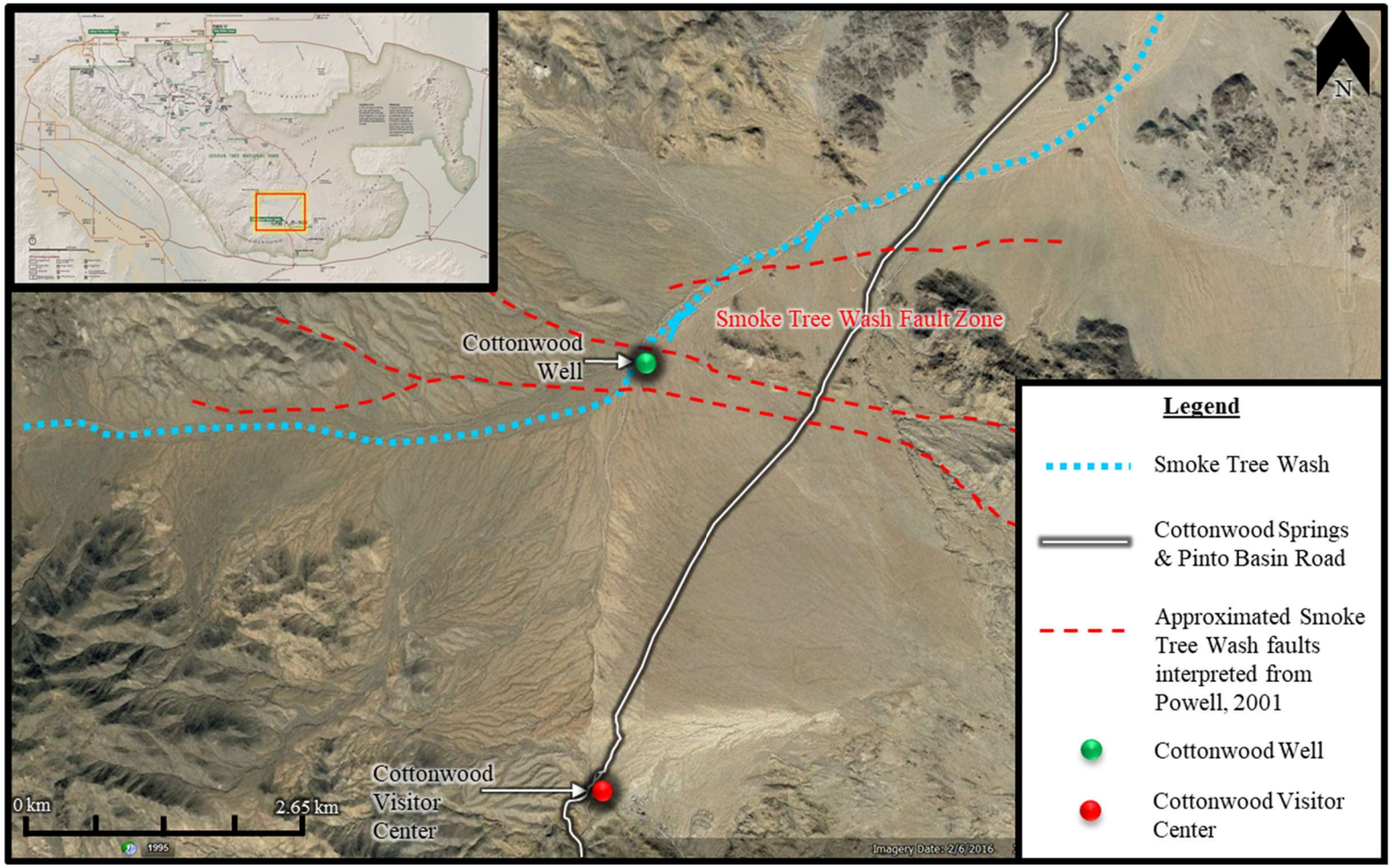

Figure 1-4. Smoke Tree Wash Orientation with approximated faults indicated (Powell, 2001)

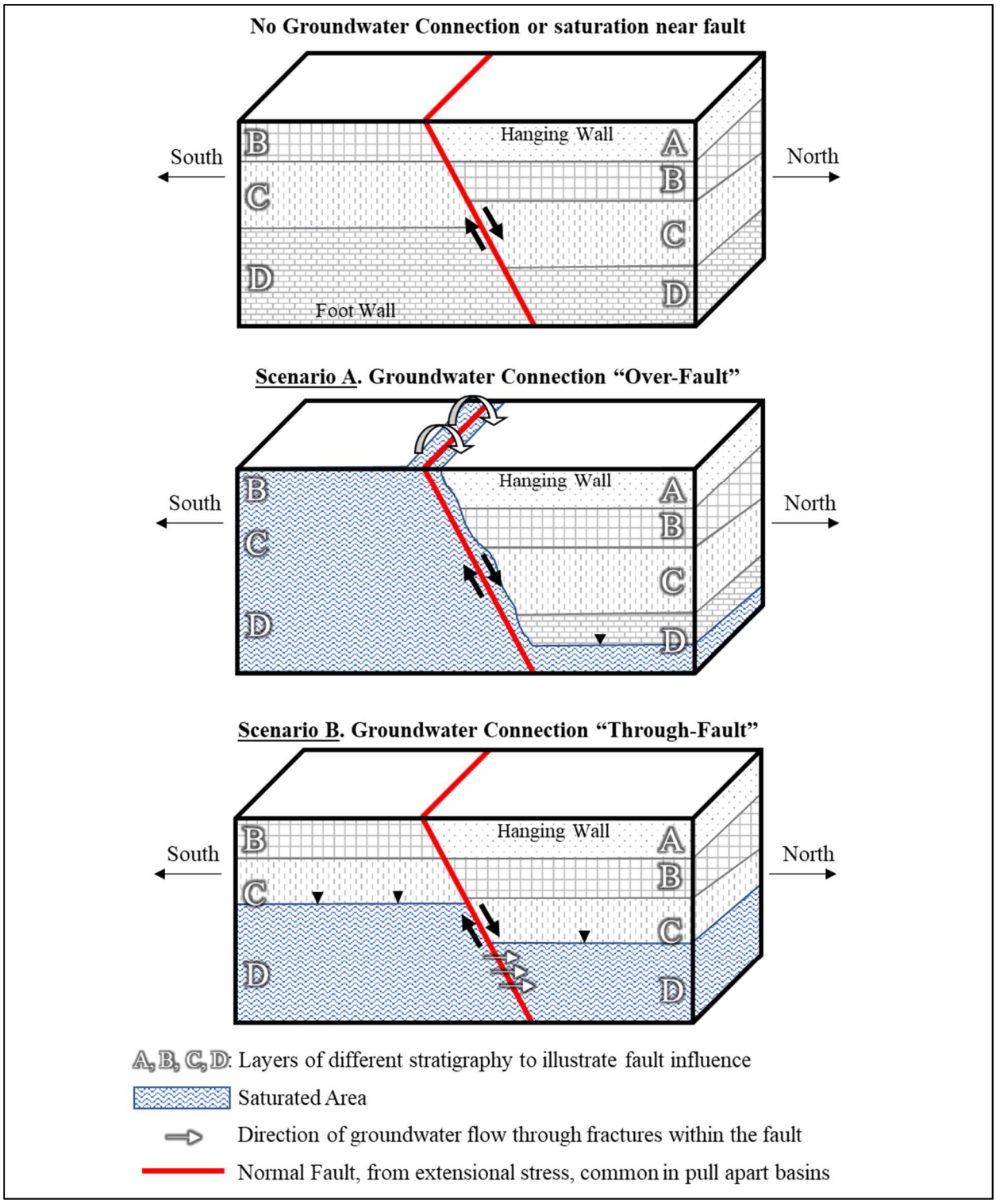

Figure 1-5. Fault-Controlled groundwater connection concept. Conceptual illustrations of a fault-controlled groundwater connection also known as a fault-controlled spillway. Scenarios are: no groundwater connection [top], over-fault groundwater connection [middle], or through-fault groundwater connection [bottom].

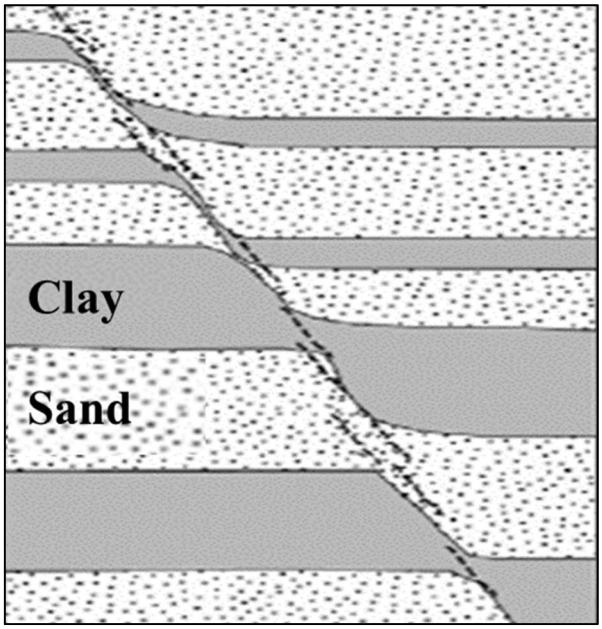

Figure 1-6. Fault architecture in faults with soft-sediment deformation at shallow depths
Source Credit: Heynekamp et al., 1999.

2. BACKGROUND

2.1 Site Description

JOTR is located in southern California bordering the Mojave and Sonoran deserts (Figure 2-1) of the Transverse Ranges in California (Powell, 2015). The principal basin of JOTR is the Pinto Basin and within the Pinto Basin there are several sub-basins. Key contributing studies in JOTR have combined several sub-basins and have referred to them as the Joshua Basin Water District (JBWD). However, for clarity, this study only focuses on the interaction between the Cottonwood sub-basin and the Pinto Basin (Nishikawa et al., 2004). The principal area of interest for this study is the Cottonwood sub-basin on the southcentral fringe of the Pinto Basin (Figure 1-3) underlying ~8,900 hectares (~22,000 acres) of the park. In most studies, the Cottonwood sub-basin is included in and referred to as the Pinto Basin. Only in more recent studies has it been identified as a research area of interest and labeled as the Cottonwood sub-basin. It is bounded on nearly all sides by the Eagle Mountains to the east, Hexie and Cottonwood Mountains to the north and west, and the Cottonwood Mountains to the south (Figure 2-2). We assume, similar to Karst & Rice's (2018) conclusions, that these mountain boundaries isolate the Cottonwood sub-basin from any other groundwater system to the south or west. The potential fault-controlled spillway identified by Karst & Rice (2018) is in the northeast area of this sub-basin.

This research found a relief of approximately 24m per km in the center of the Cottonwood sub-basin and leveling off significantly to the northeast at a gradient of 8m per km. These findings are consistent with previous studies in the area for surface conditions. Hydrogeological analysis by Weir & Bader (1963), however, indicate a southward hydraulic

gradient for subsurface flow, until water accumulates in the deeper alluvial deposits (Weir & Bader, 1963). The totality of the field work conducted herein was located in wilderness washes or relatively flat / graded terrain at an average elevation of 900m (~2950 ft) above sea level. This supports the presumption that overland flow in washes originating in the Cottonwood sub-basin could flow into the Pinto Basin due to topographic relief. However, hydrogeologic studies indicate that once water has infiltrated the subsurface outside of the wash, it will be retained in the Cottonwood sub-basin (Weir & Bader, 1963).

2.2 Geologic setting

The Cottonwood sub-basin is part of the Pinto Valley which is mainly comprised of alluvium (Kunkel, 1963). The deposits in this valley vary in ages from Precambrian to Quaternary. The alluvial and lacustrine deposits consist mainly of clay, silt, sand, and gravel with interbedded basalt at greater depths (Scharf, 1935). The mountains, that act as natural boundaries for subsurface flows, are a mix of Jurassic and pre-Cretaceous aged rock and are predominantly igneous (granitic) (Jenkins, 1938). The presence of fractures or evidence of any underflows (aside from the Cottonwood Springs outflow) have yet to be defined for this area.

Geologic formations in the area of the Cottonwood sub-basin can be divided into nine stratigraphic layers. From oldest to youngest these layers are: basement complex, old alluvial deposits, olivine basalt, Pinto formation, older alluvium, lacustrine deposits, younger alluvium, playa deposits, and sand (Weir & Bader, 1963). The basement complex is likely Precambrian metamorphic rock intruded by igneous rock (Miller, 1938). Old alluvial deposits are inter-layered silt and sand units. The olivine basalt is in places interbedded with the old alluvial deposits and where exposed tends to be vesicular. The Pinto formation is composed primarily of Pleistocene lacustrine deposits. The maximum thickness is unknown, but it has been suggested

by Scharf (1935) there are at least two primary layers, 45 meters of sedimentary deposits and 45 meters of interbedded basalt, displaced by faulting (Scharf, 1935). The older alluvium layer is interbedded by lacustrine and clay deposits and is displaced by faulting and deformed by folding with an estimated thickness of ~57m (~187ft) between depths from surface of ~16-74m (~51-243ft) (Weir & Bader, 1963). The lacustrine deposits that overlie the older alluvium consist of poorly sorted sand, silt, and clay. Younger alluvium is very shallow and is either only a few meters thick, or not present in some areas between the most recent playa deposits. The playa deposits and sand are very thin layers that sit as the most recent layer of deposits. No permanently saturated areas are known to exist above the lacustrine deposits (Weir & Bader, 1963). The stratigraphic interpretation of Weir & Bader is consistent with the driller's logs of LUB-23 taken in 1958 (Figure 2-2). However, it must be noted that the depth of the Cottonwood sub-basin varies greatly and most depths are estimated and not known due to lack of studies in the area.

LUB-23 was drilled in 1958. The original driller's log refers to LUB-23 as well 4S/11E-27Q (Cottonwood Pass Well). These logs (Table 2-1 & Figure 2-3) subdivide the stratigraphy into three main categories: younger alluvium, older alluvium, and basement complex. This early estimate is similar to the nine subdivisions determined by Weir & Bader (1963). Younger alluvium is reported to be approximately 18m (60ft) thick with older alluvium consisting of mostly boulders and clay with a thickness of 47m (155ft) reaching a total of 65m (215ft) bgs. The well extends into what they refer to as a basement complex consisting of boulders, clay, and gravel reaching a total depth of 122m (403ft) and is perforated from ~63m-122m (~208 – 403ft) (Weir & Bader, 1963).

Scharf suggests that principal volumes of water are stored in the older alluvium layer and in the interbedded Pinto formation (Scharf, 1938). In 1963 the groundwater level in LUB-23 was at a static level of 51m (170ft) bgs and the zone of saturation was estimated to be about 71m (233ft) thick (Weir & Bader, 1963). The most recent water budget computation to include an estimated groundwater storage capacity was conducted for the Cottonwood sub-basin in 2018 by the National Park Service (NPS). Based on varying reported groundwater levels, the range of storage capacity was estimated to be between $0.07km^3$ and $0.10km^3$ (56,000 ac-ft and 84,000 ac-ft) (Karst & Rice, 2018). Potential outflows are estimated to be evapotranspiration, groundwater extraction, and subsurface outflow (via fault-induced springs) that result in a change of storage between $1973m^3/yr$ and $2837m^3/yr$ (1.6 ac-ft/yr and 2.3 ac-ft/yr) (Karst & Rice, 2018). The high end of the estimated change in storage (which includes all outflows) would not result in the observed water level declines of more than ~15m (49ft) if outflows were limited to evapotranspiration, legitimate groundwater extraction, and identified spring outflows. There has been no evidence of illegitimate groundwater extraction in the Cottonwood sub-basin of Joshua Tree National Park, and is assumed not to be an influence for this study.

2.3 Faulting & Seismic Activity

Since the North American Plate and Pacific Plate are both made of continental rock and similar density, neither will subduct below the other (Trent & Hazlett, 2002). With no subduction these two plates slowly negotiate around each other by sliding past, creating the San Andreas Fault. This one large fault sets conditions for zones of faulting throughout the area in addition to pull apart basins as a result (Aydin & Nur 1982). Networks of faults are common in the Mojave Desert and many existing fault-bounded sub-basins have large variance in water levels (Bedrosian et al., 2013). Second only to the San Andreas Fault, the Pinto Mountain Fault is one

of the most prominent faults in the JOTR area and is located at the northern edge of the Pinto Basin (Trent & Hazlett, 2002). For comparison from another study, evidence shows the Pinto Mountain Fault separates the Copper Mountain sub-basin (CMSB) from the Pinto Basin. Elevation at CMSB is lower than the Pinto Basin and depth to water in the Copper Mountain sub-basin has a depth to water 21-30m (70-100ft), below the surface of the Pinto Basin (Lewis, 1972). Thus, similar to the Copper Mountain sub-basin relationship with the Pinto Basin, we would expect to see distinct variance in groundwater levels in the research area between the Cottonwood sub-basin and the larger Pinto Basin being fault separated basins. In this study, the Cottonwood sub-basin sits at higher elevation than the neighboring Pinto Basin to the northeast and it's possible that fracturing in inferred faults has created an avenue for groundwater to flow into the Pinto Basin. Water table elevation at LUB-23 is 842m above sea level, and the surface elevation of the Pinto Basin is 865m near the boundary of the two discussed basins. In the general research area, the Porcupine Wash and Smoke Tree Wash faults (Figure 2-2) are the primary east-west oriented faults. The Porcupine Wash fault is approximately 4.3km (2.7 miles) north of the Smoke Tree Wash fault zone, and not relatively influential to a relationship between the Cottonwood sub-basin and the Pinto Basin. The Smoke Tree Wash fault zone does have the potential to be a direct influence on groundwater connection between the Cottonwood sub-basin and the Pinto Basin. Thus, it is the primary zone considered in this study. The Smoke Tree Wash fault zone has three primary faults running east to west, likely a system of dip-slip or extensional normal faults, consistent with being a pull-apart basin (Powell, 2001). Additional faulting is most evident on the northern edge of the Eagle Mountains (south of this study area), and is characterized by an eastward oriented scarp (Kunkel, 1963). Despite a hydraulic gradient that brings subsurface waters to aggregate in the alluvial deposits, Weir & Bader (1963) suggest that

groundwater from the Cottonwood sub-basin could move slowly through or over the fault zones northeastward into the Pinto Basin due to a localized change in hydraulic gradients induced by faulting (Weir & Bader, 1963). This is a substantiating rationale for the purpose and scope of this research. Besides groundwater extraction the only groundwater outflow that has been identified conclusively is from the fault zones that contribute source waters for springs. Fault-zones can allow groundwater to rise on the upslope side of the fault and this occurs at the Cottonwood Springs as the only known outflow besides groundwater extraction (Trent & Hazlett, 2002).

Valley fill depth interpretation from gravity data is imposed over the outline of the Cottonwood sub-basin to show depth and shape of the basin (Figure 2-5), suggesting that the Cottonwood sub-basin (in vicinity of the Smoke Tree Wash) is a pull apart basin (Langenheim, 2016). Factors that contribute to this are: (1) length is twice its width, (2) depth greater than 100m, and (3) basin length oriented in the same direction of the Smoke Tree fault (Aydin & Nur, 1982). Continual evolution of pull apart basins can develop separate faults being joined to create a larger basin. This potential for complex fault system interaction is the rationale for investigating the potential presence of a fault-controlled spillway, as discussed later in the background section.

Similar sub-basins in JOTR are fault-bounded. Three specific examples include the Copper Mountain sub-basin, the Warren sub-basin, and the Twenty-nine Palms sub-basin. All three sub-basins have water level elevations that are higher than the water elevations in the Pinto basin that it borders, by hundreds of feet (Nishikawa et al., 2004). Dissimilar to the Cottonwood sub-basin, there is a greater potential in these sub-basins to have groundwater connections because saturated depths are close to the boundaries between the basins. In the study area, valley fill depth and saturated thickness of the Cottonwood sub-basin is more than 2km away from the

boundary. However, in these three sub-basins the faulting has caused deformation and cementation which can create barriers to flow (Nishikawa et al., 2004). The similar concept could be applied to the Cottonwood sub-basin and this study investigates whether or not a groundwater connection could exist through a potential barrier to flow. Additionally, this will help contribute to understanding characteristics of the sub-basin that inform a more refined water budget, particularly since there is limited hydrogeologic information in the study area as compared to the Northern part of the park (where the Copper Mountain, Warren, and Twenty-nine Palms sub-basins are located).

If there has been a groundwater connection via a fault-controlled spillway between the Cottonwood sub-basin and the Pinto Basin, it is likely that it has existed since before LUB-23 was installed in 1958. Therefore, it would not be a new underflow just an undocumented underflow. However, albeit the unlikely scenario, it is possible that recent seismic activity has induced fractures or avenues of groundwater flow between the basins. According to the USGS earthquake monitoring service, JOTR has experienced more than 500 earthquakes in the last year. The largest earthquake of recent time has been a 7.3 magnitude earthquake in 1992 (USGS, 2019). The amount of seismic activity and tectonic movement in the region could be contributors to creating fractures or avenues to provide groundwater connections between basins.
An objective of this study is to identify the presence or lack of a groundwater connection which could be attributed to fractures in a fault between the basins, but this study is not investigating the cause, only the presence.

2.4 Hydrogeology

Precipitation is the only source of recharge to the Cottonwood sub-basin. According to the Western Regional Climate Center (WRCC), JOTR has an average high temperature of 26.4°

C (79.6° F) and an average low of 10.6° C (51.2° F) with the hottest months of July and August averaging over 37.8° C (100° F). Classified as an arid climate, precipitation data lists an annual high average of 207mm (8.18”) and an annual low of 59mm (2.33”) from data collected 1959 through 2012 (WRCC, 2019). Only 21 total days of calendar year 2018 experienced precipitation. These amounts totaled 180mm (7.1”) at the Joshua Tree 2.0 Weather Station, (~60km from the research study area) with 59mm (2.34”) of precipitation coming in one event on 13 October 2018 (6 weeks prior to data collection for this research) according to the National Oceanic & Atmospheric Administration (NOAA). Groundwater recharge is predominantly from precipitation during the winter months (January-February 2018; November-December 2018) but, in 2018 precipitation only totaled 57mm (2.25”). Thus, precipitation events vary greatly year to year and water levels may be sensitive to these variations. It is important to note, however, variations in precipitation occur greatly within the park itself due to elevation. According to data from 2006-2017, average annual precipitation recorded by the Cottonwood Canyon station is approximately 114.3mm (4.5 inches) of precipitation annually (Karst & Rice, 2018). The Cottonwood Canyon meteorological station (KCAEAGLE) is no longer in service as of January, 2018. There are no current precipitation stations that provide specific data, but it has been suggested that southern areas of the park when receiving 50-76mm (2-3”) of rain will have rains of 101-127mm (4-5”) in the northwestern area of the park (Weir & Bader, 1963). Therefore, official climatic precipitation values may overestimate the cumulative value of precipitation for this area of interest.

There are no perennial streams or bodies of water in the Cottonwood sub-basin. However, the area is prone to flooding when high intensity or long-term precipitation events occur in the mountains. These events result in the washes that are evident in the topography of

the area (Campbell & Campbell, 1935). The frequency and location of playas in this area of JOTR has not been documented but the area does have a history of known playa deposits (Weird & Bader, 1963).

Two different depths to water were used in conjunction with estimated depths to bedrock (from gravity data) to estimate storage capacity in Karst & Rice's 2018 water budget model of the Cottonwood sub-basin aquifer (Karst & Rice, 2018). The range of depth was estimated using seismic data (depth to water 51m or 170ft bgs) and the observed depth to water (67m or 219ft) to determine storage potential (Langenheim et al., 2016). Thus, $1.0x10^8m^3$ and $6.9x10^7m^3$ (84,000ac-ft and 56,000ac-ft) is the estimated storage when assuming the sub-basin is primarily sand and gravel with drainable porosity as is understood from known stratigraphic analysis. Karst & Rice (2018) assumed a specific yield value of 0.15 in their calculations (Karst & Rice, 2018).

Natural recharge in JOTR as a whole to include the Cottonwood groundwater sub-basin is limited. Besides potential recharge underflow the only source of ground water in the Cottonwood sub-basin is precipitation. Infiltrating water percolates through the pores to the water table (Kunkel, 1963). Recharge to the Cottonwood sub-basin is derived mostly from runoff from the precipitation events over the encircling mountain ranges via infiltration and is estimated to be approximately 11.4cm (4.5in) annually for calculations. Total recharge estimates were determined through two methods. First, using groundwater modeling estimates from a 2004 study combined with the approximated area of the Cottonwood sub-basin; precipitation indicated a potential total recharge between $1.0x10^5m^3/yr$ and $1.8x10^5m^3/yr$ (85-150 ac-ft/yr) (Karst & Rice, 2018) (Nishikawa et al., 2004). The chloride mass balance (CMB) method was used as a second estimate suggesting recharge was between $7.4\ x10^4m^3/yr$ - $1.0x10^5m^3/yr$ (60-85ac-ft/yr)

(Karst & Rice, 2018). The CMB is a tracer technique used to estimate groundwater recharge under steady-state conditions by comparing total chloride deposition from the surface to the concentration in groundwater (Naranjo et al., 2015). When recharge rates are low in comparison to total precipitation (due to the overland flow of the local washes) CMB is generally more reliable than the water balance method (Scanlon et al., 2002). One additional inflow includes septic return, estimated to be approximately 2100m^3/yr (1.7ac-ft/yr) (Karst & Rice, 2018). Ultimately, the lowest estimate and highest estimate will be used for the range of annual recharge to the Cottonwood sub-basin: 7.4 x$10^4$$m^3$/yr – 1.8x$10^5$$m^3$/yr (60-150ac-ft/yr) (Karst & Rice, 2018).

Spring outflows at the Cottonwood springs are estimated to be 3700m^3/yr (3ac-ft/yr). (Sada & Jacobs, 2008). Groundwater extraction averaged over 2015 and 2016 was 4934m^3/yr (4ac-ft/yr) (Karst & Rice, 2018). Evapotranspiration is estimated to be 3700m^3/yr (3ac-ft/yr), campground and recreational use is estimated to be approximately 2700m^3/yr (2.2ac-ft/yr), and employee housing is estimated to be 1600m^3/yr (1.3ac ft/yr) (Karst & Rice, 2018). Although it is assumed that there are no subsurface inflows into the Cottonwood sub-basin, it is assumed that there is 7.0 x$10^4$$m^3$/yr – 1.8 x$10^5$$m^3$/yr (57-147ac ft/yr) as subsurface outflow. This large amount would replicate conditions we see over time. Without this large outflow, the aquifer water table would be rising over time. Including this assumed value, we see a decline in about 2800m^3/yr (2.3ac/ft yr). However, it is unknown the avenue this outflow takes. A full water budget accounting authored by Karst & Rice (2018) is seen in Table 2-2.

Park personnel report that the water level has declined in the LUB-23 well from 51m (170ft) bgs when it was installed in 1958 to about 67m (219ft) bgs over the last few years. The reason for this decline can only be speculated at this point since groundwater extraction and

spring discharge would not cause this decline on its own (Karst & Rice, 2018). Poor well screen conditions, faulting losses, and interbedded impermeable layers (clays) could contribute to a larger cone of depression around the well or aggregate water declines (Karst & Rice, 2018). Our research focused on investigating groundwater connections between the Cottonwood sub-basin and the Pinto Basin in order to better characterize the hydrogeological relationship at the boundary.

2.5 Previous research and data collection

Numerous studies (Nishikawa et al., 2004, Kunkel, 1963, Weir & Bader, 1963, Mathany et al., 2012, and Bedrosian et. al, 2013) have been conducted with respect to groundwater flow, basin evolution, and geologic setting for the entirety of the Joshua Tree National Park, but limited information is available specifically tailored to the Cottonwood sub-basin and the relative interaction of groundwater with its geologic surroundings. The earliest primary investigation inclusive of the Cottonwood area was by Weir & Bader in 1963. Water source reconnaissance was conducted by Mendenhall in 1909 that investigated and documented outflow of Cottonwood Springs (Mendenhall, 1909). In 1912, Harder investigated the Eagle Mountains and further documented Cottonwood Springs (Harder, 1912). In 1935 Scharf investigated the geologic units in the area with an archeological study of Pinto Basin (Campbell & Campbell, 1935). Unpublished reports from J.V. Lewis in 1941 and 1942 documented the alluvial deposits in the area and Kunkel conducted a hydrologic and geologic reconnaissance of Pinto Basin in 1960 (Kunkel, 1963).

In 2000, the U.S. Geological Survey (USGS) began groundwater flow studies in JOTR, but focused on the relationship between the Copper Mountain sub-basin and the Joshua Basin Water District at large (Nishikawa, et al., 2004). Additional NPS and USGS data collection

efforts concentrated on water quality data such as the baseline data collected in 2001 by the NPS and groundwater quality data by the USGS in 2009 (Mathany, et al., 2012). Powell in conjunction with the USGS has conducted the most extensive work, mapping the geological characteristics of JOTR for over ten years with such contributions as the current Porcupine Wash 7.5° quadrangle geologic map (Figure 2-6), fault zone maps, and a geodatabase for reference (Powell, 2001 & 2015). A 2013 study focused on the Pinto Mountain Fault and varying depth to water measurements on either side (Bedrosian, et al., 2013). Using time domain electromagnetic (TDEM) inversion, this study investigated hydrogeological characteristics of the fault zone in the northern part of JOTR. Although TDEM is distinctly different from ERT, using means of electrical investigation in the aridity of Joshua Tree appears to be reliable. This particular study attempted to use a 600m long ERT survey, but data was considered unreliable when they were plagued with high contact resistance (Bedrosian, et al., 2013). This result prompted the preparation to improve contact resistance, which was accomplished using a localized salt water solution around electrodes.

Of particular importance to this study to interpret an alternate well location was isostatic gravity gradient data and seismic refraction data for the Cottonwood sub-basin. The isostatic gravity data from Langenheim et al., 2016, consisted of 89 individual measurements using an absolute gravimeter that contributed to constructing that valley fill depth interpretation. Seismic refraction data (discussed later) also collected by Langenheim et al. (2016), was instrumental in interpreting the resistivity data, and confirming depth to water readings. This was collected along the relatively same path as one of the ERT surveys (Survey A) and extended 1100m providing a seismic interpretation which we compliment with the resistivity data.

This research is in response to the need identified by the USGS and NPS for further geophysical investigation of the boundary conditions between the Cottonwood sub-basin and the Pinto Basin (Karst & Rice, 2018).

Table 2-1. Driller's logs for LUB-23, source credit: Weir & Bader, 1963. Within the source credit LUB-23 is referred to as the Cottonwood Pass Well (4S/11E-27Q1).

Description		Thickness (ft)	Total Depth (ft)
Younger Alluvium			
	Sand, gravel	60	60
Older Alluvium			
	Boulders, clay content	55	115
	Sand, clay content	20	135
	Clay, boulders	43	178
	Clay, pure	5	183
	Boulders, clay, very rough, water	32	215
Basement Complex (?) residuum			
	Boulders, clay	16	231
	Gravel, boulders, clay	54	285
	Soft, probably more water	20	305
	Clay, some gravel	98	403

Table 2-2. Cottonwood sub-basin water budget. Source Credit: Karst & Rice, 2018.

		Low Recharge Estimate	High Recharge Estimate
Groundwater Inflows (ac-ft/yr)			
	Recharge from Precipitation	60	150
	Subsurface Inflow	0	0
	Septic System Return Flow	1.7	1.7
	Subtotal	61.7	151.7
Groundwater Outflows (ac-ft/yr)			
	Evapotranspiration (ET)	3	3
	Groundwater Extraction		
	• Visitor Center	2.2	2.2
	• Employee Housing	1.3	1.3
	• Campground / Irrigation	0.5	0.5
	Subsurface outflow	57	147
Change in Groundwater Storage (ac-ft/yr)		-2.3	-2.3

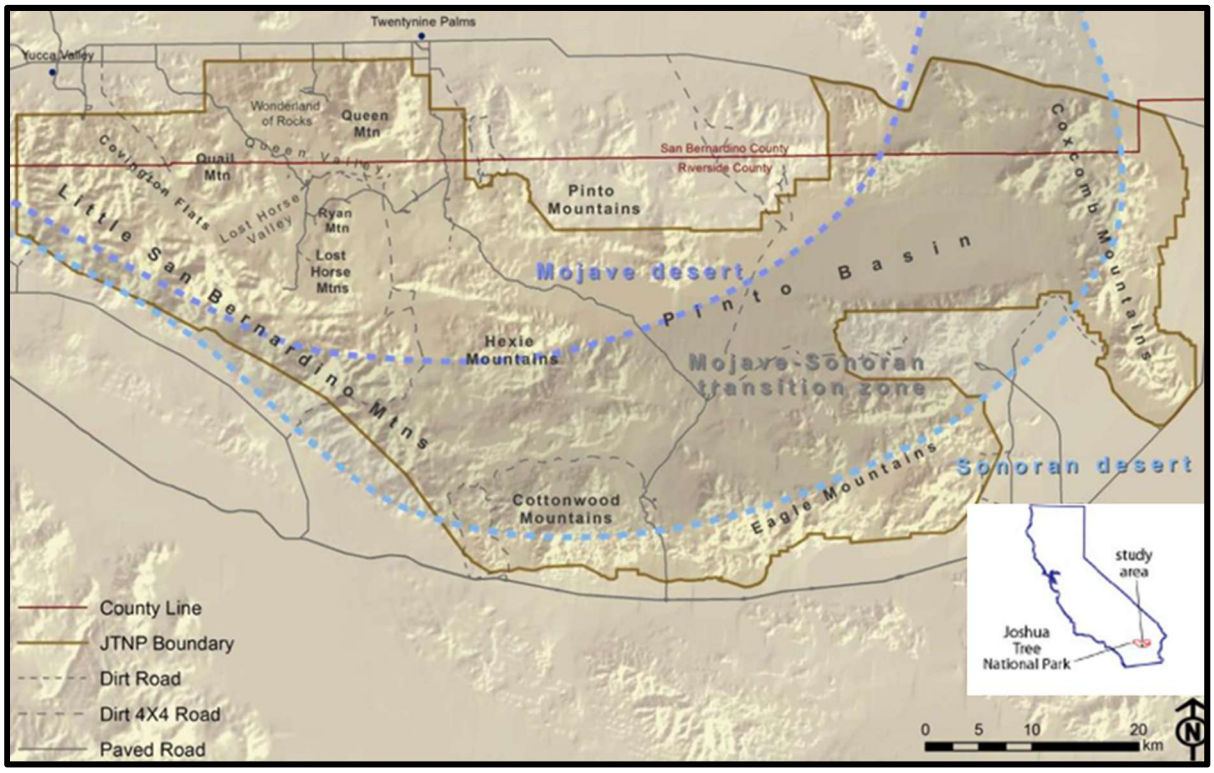

Figure 2-1. Joshua Tree National Park Desert Boundaries. Relation to the Mojave & Sonoran deserts. Modified from source credit: National Park Service, Mitzi Harding.

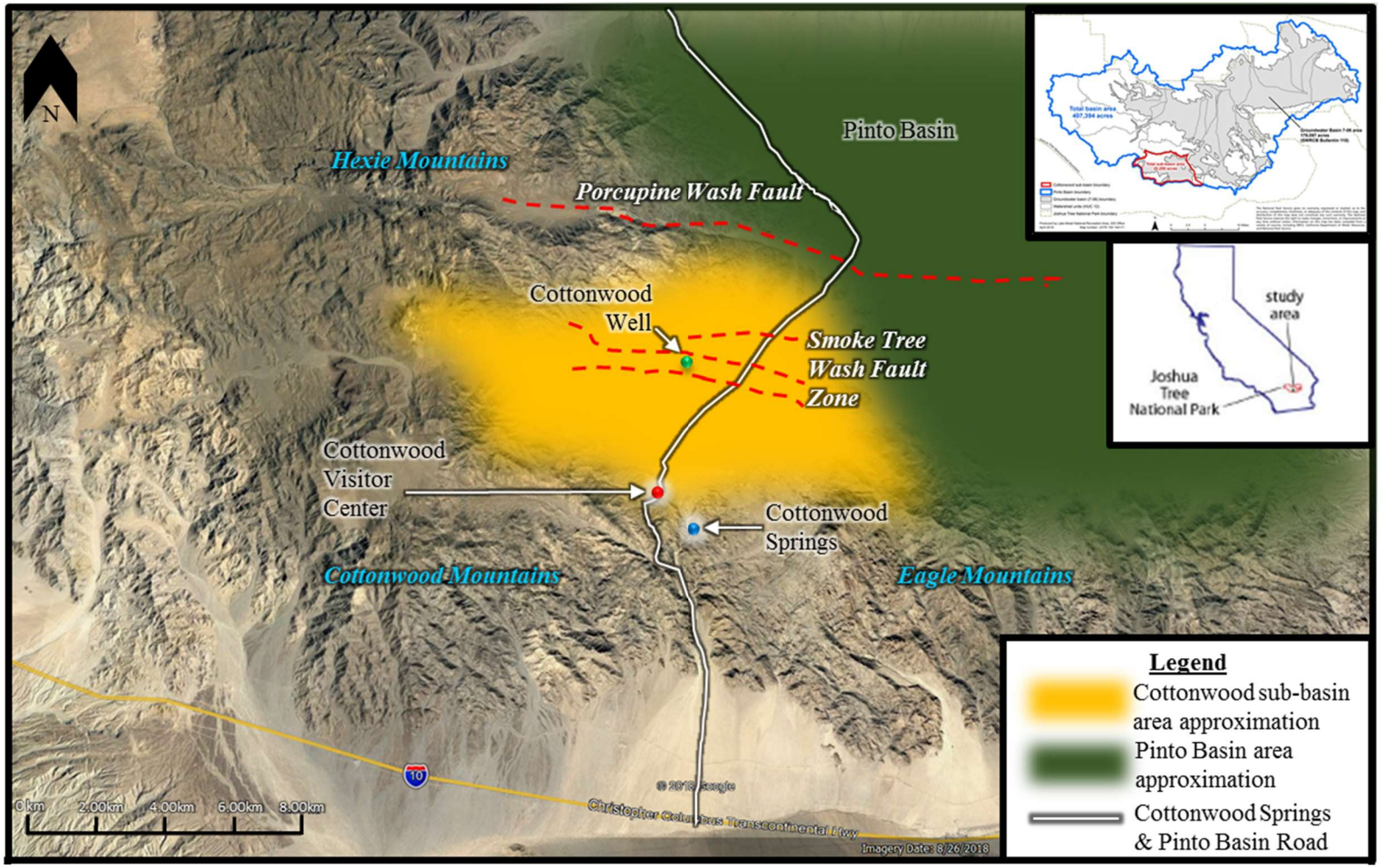

Figure 2-2. Basin & Fault Orientation. Cottonwood sub-basin area approximation interpolated from Powell, 2001 and National Park Service – Lake Mead National Recreation Area GIS Office, April 2018 Map # JOTR 156 144170.

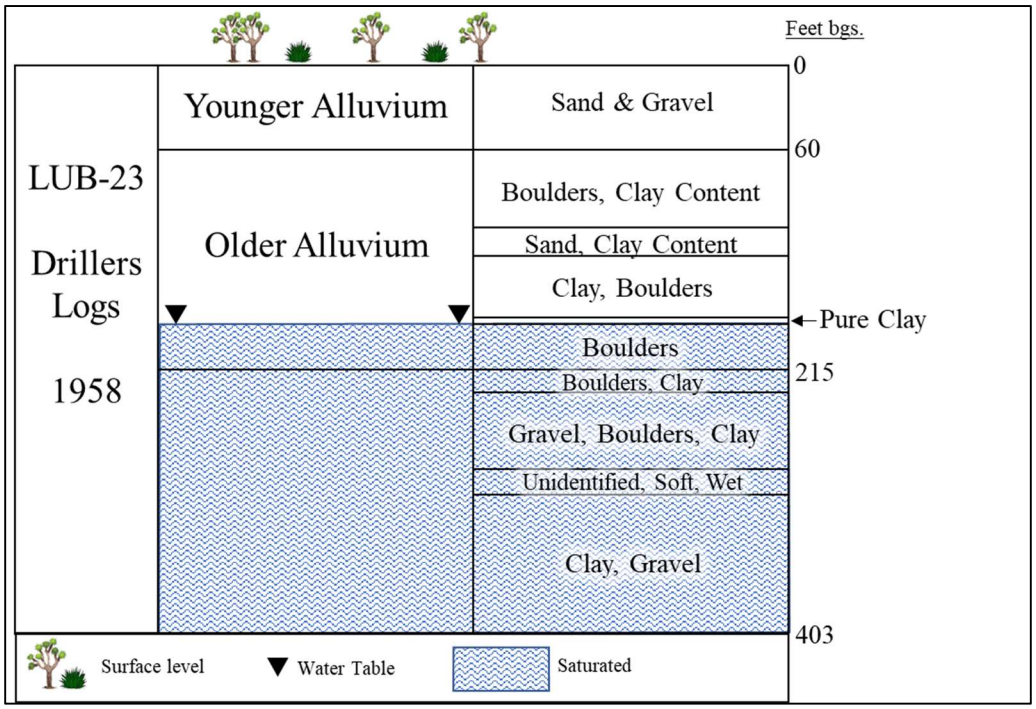

Figure 2-3. Estimated stratigraphy illustration interpreted from driller's logs of LUB-23, refer to Table 2-1 for complete description and depths.

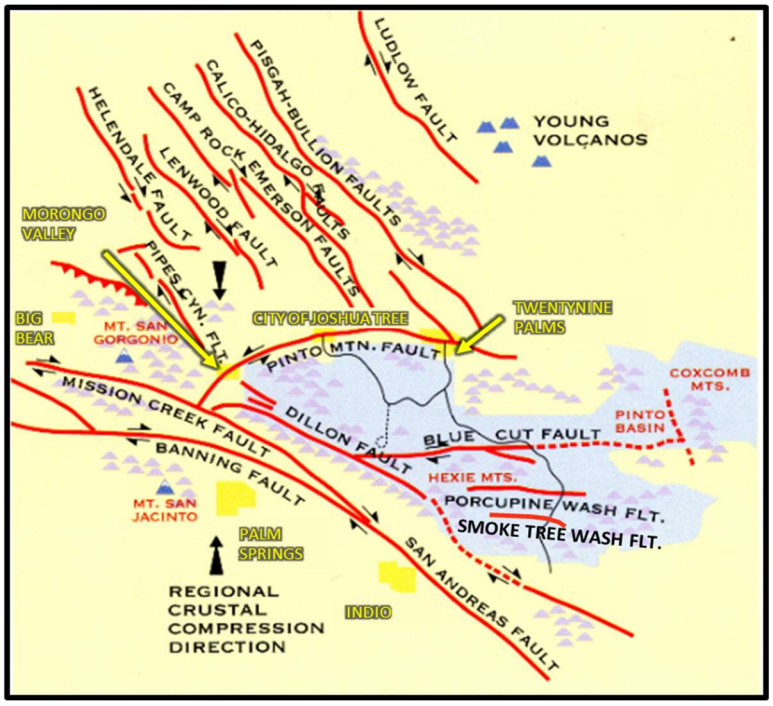

Figure 2-4. Faulting in southern California. Illustration modified from source (Trent & Hazlett, 2002). Smoke Tree Wash Fault Zone and the Cottonwood sub-basin are directly south of the Porcupine Wash Fault.

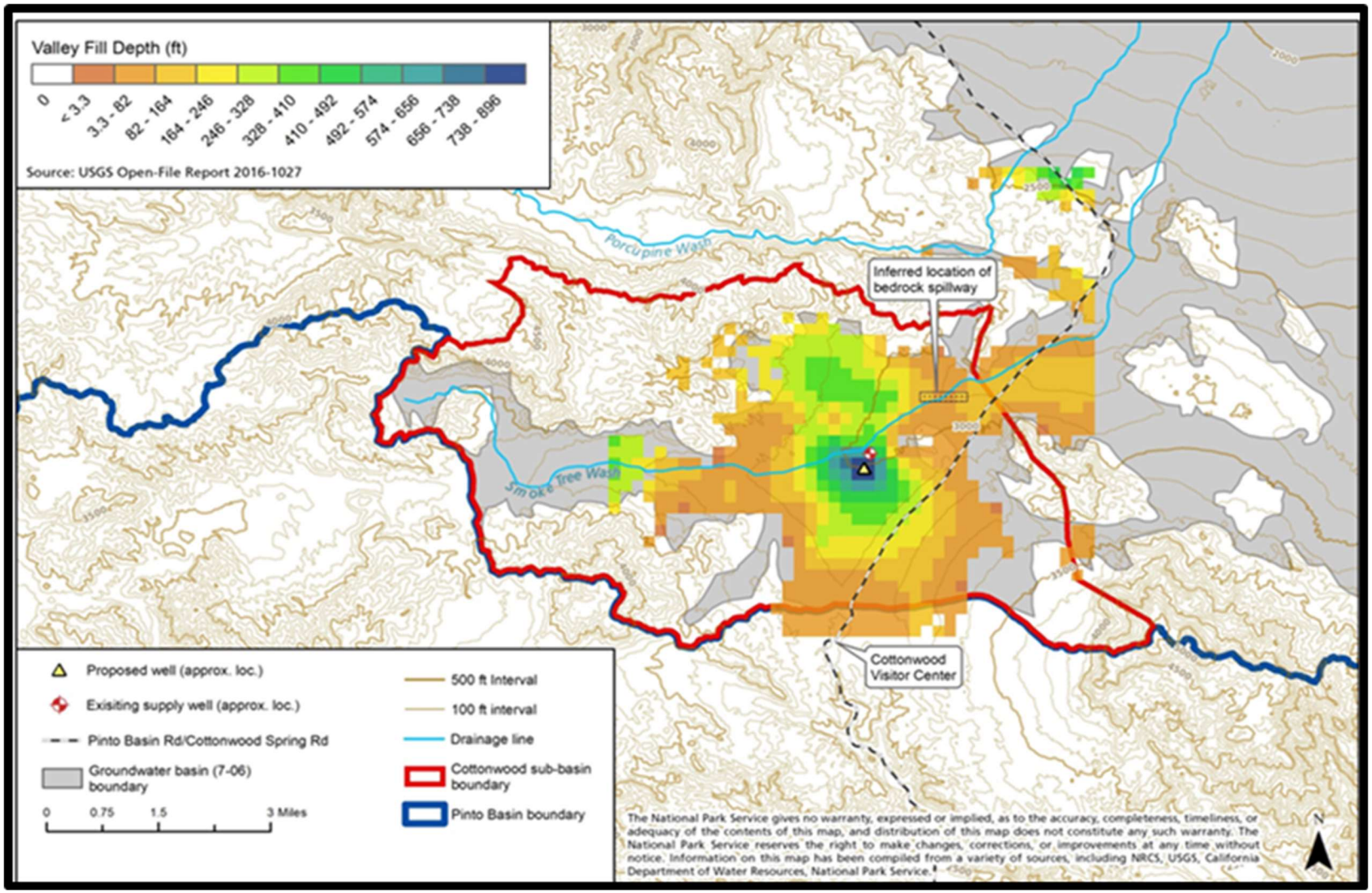

Figure 2-5. Valley Fill Depth. Valley fill depth estimated from the gravity data and an inferred location of a bedrock spillway in the Smoke Tree Wash fault zone. Source credit: National Park Service – Lake Mead National Recreation Area GIS Office, April 2018 Map # JOTR 156 144170

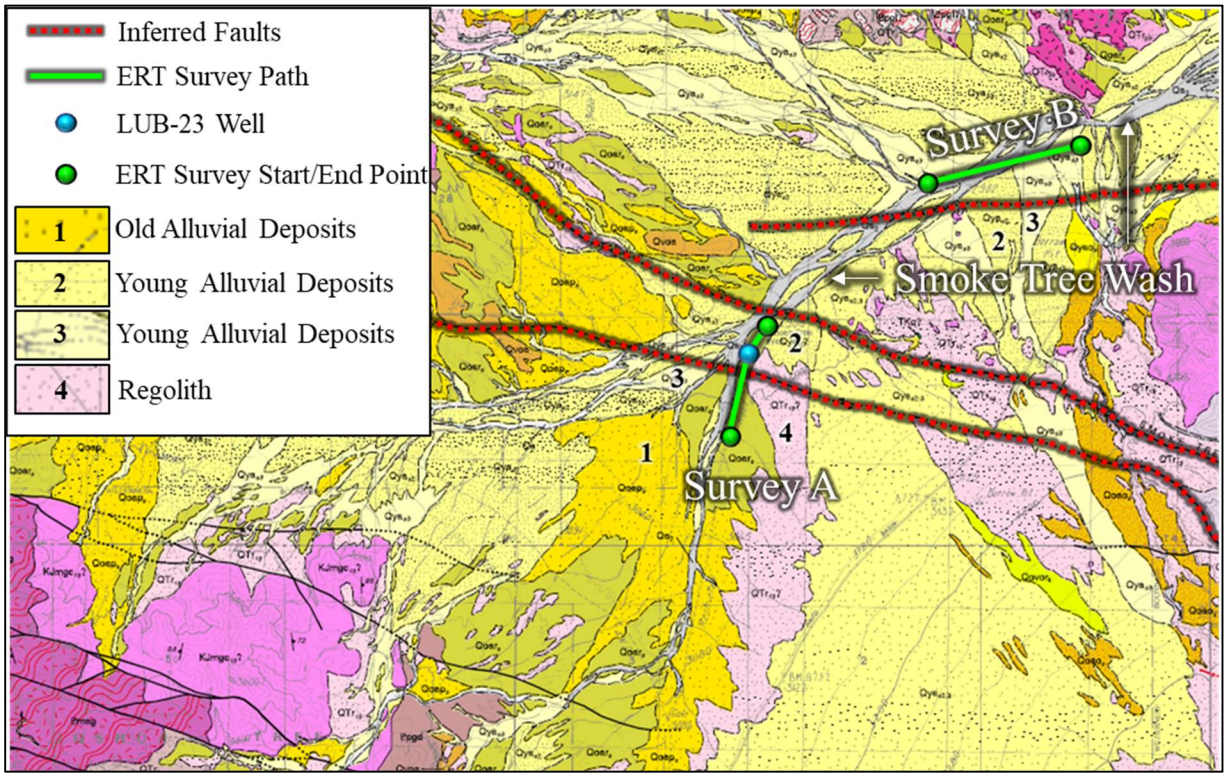

Figure 2-6. Geological Map: Porcupine Wash 7.5° quadrangle map authored by Powell, 2001. Source credit: Modified from the USGS geologic quadrangle map at: https://pubs.er.usgs.gov/publication/ofr0130

3. METHODOLOGY

This study has four objectives (1) investigate groundwater connections between the Cottonwood sub-basin and the Pinto Basin, (2) investigate causes of potential inefficiency of LUB-23, (3) conduct water quality analysis, and (4) validate the NPS recommendation for a secondary well. These objectives will be accomplished using three primary methodologies. Direct current (DC) electrical resistivity tomography (ERT) was used to map subsurface resistivity characteristics of the Cottonwood sub-basin for objectives (1) and (4). Depth to water in LUB-23 was determined by visual confirmation with a snaking camera and confirmed with a well sounder while investigating objective (2). The potential inefficiency was partially assessed from camera observations, a well sounder, and brief pump test. Appendix 3 includes field data collection photos. For objective (3), geochemical analysis commercial off the shelf (COTS) probes were used to determine well water temperature, pH, dissolved oxygen and specific conductance. Hach method 8203 was used to determine alkalinity and water samples were collected to determine general chemistry and stable isotope values through requisitioned lab analysis.

3.1 Electrical Resistivity Tomography (ERT).

Gravity and seismic geophysical techniques have been used previously in the Cottonwood sub-basin area, in a complimentary approach for this study. Electrical resistivity (ER) provides a high-resolution image of subsurface characteristics at smaller scale and is a technology made available by the National Park Service for use in this research. Since ERT has not been used in this area previously, it provides reinforcing data to corroborate the findings from the gravity and seismic data. In addition to being minimally invasive, ERT has been proven

successful from other similar studies for: (1) arid climates, (2) investigating fault zones, and (3) depth to water investigations (Ammar, et al., 2018). Since we are trying to replicate investigative success of those three characteristics, ERT was chosen as the technology for investigation.

ERT consists of the raw data from ER combined with interpretive analysis to create a model illustrating subsurface characteristics. ER measures the potential of subsurface materials to resist electrical flow by injecting low frequency electrical currents into the ground and measuring the values of resistance to the current in Ω (ohm) meters through the electrical path (Brinley, 2015). Electrical resistivity is determined by how the properties of the material affect the ratio of voltage potential compared to electrical current (Reynolds, 1997). An inversion algorithm to an inverse problem is then solved to illustrate a model correlated to the data (Oldenburg and Li, 1999). Basically, the resistivity (R) multiplied by the currents (I) that were passed between electrodes equals the potential difference (V). This is also referred to as Ohm's Law or V = (I) * (R). With ERT we will inject a current, measure the difference, and it will provide the subsequent resistivity of the subsurface. Inversion is the process of mapping how the subsurface resistivity is distributed from collected data to understand subsurface geology (with a close correlation). The results of the data collection plus the model illustration is considered ERT or a subsurface tomographic model. Since, high resolution and accurate data are desired, two key concepts were taken into consideration to determine the setup and execution of the arrays. The first concept, depth of investigation (DOI), defines a depth that is considered to be interpretively accurate and ultimately drove the design for electrode spacing and survey length. Advanced Geosciences Inc. (AGI) indicates that accurate data can be acquired at a depth 20% of the survey length (AGI, 2009). The second concept, array execution is how the injected current is applied and measured from the physical setup of electrodes. This can be accomplished by using an

electrical resistivity meter which sends electrical currents into the ground and measures the resulting potential, providing a resistivity measurement in Ωm. This study utilized the Advanced Geosciences Incorporated (AGI) manufactured Supersting^{TM}. These concepts working together were optimized to yield the greatest depth of data with the highest possible degree of accuracy.

The AGI Supersting^{TM} is an electrical resistivity meter used to scan an image of the subsurface of the earth with the ability through applied software to visualize the results (Supersting^{TM}, 2019). The Supersting^{TM} used for this study was the version model R8. R8 refers to the number of channels that the receiver can use at once, therefore making it a multi-channel capability. The number of channels reduces the amount of time for the selected array to be completed. For instance, with 8 channels one array can be run on each channel, thus, over thousands of iterations, the number of channels reduces the amount of time it takes to collect data. The layout of equipment required for this study was: 2x deep cycle marine batteries to power the system, 1x Supersting^{TM} Receiver, 1x switch box, 4x ERT electrode (10m spacing) land cables, 56x metal stakes, and 1x laptop (Figure 3-1). A full array consists of 4x electrode land cables extended as far as they can (560m). Each electrode land cable in this study has 14x electrode connections spaced 10m apart. Thus, each electrode land cable is 140m in length. With 4x fully extended electrode land cables, the longest array possible to be performed at once is 560m. The electrode land cables are connected to each other and the electrode cable switch box is always located in the center of the array. The switch box distributes the current through the electrode land cable and is also connected to the Supersting^{TM} which tells the switch box what to do and receives the potential measurements for data interpretation.

Measuring resistivity is accomplished by placing at least two conducting metal electrodes into the ground and passing an electrical current from one, through the ground to the next (Figure

3-3). It is necessary that the electrodes can effectively pass current, which introduces a very important characteristic of ERT to distinguish. Essential to understanding the concepts and results herein, is the difference between contact resistance and resistivity. Simplifying the two concepts, contact resistance can be seen as how well the electrode connects to the ground and how efficiently it can pass an electrical current into the subsurface. The lower the contact resistance value the better the contact. Resistivity on the other hand, is the resulting analysis of the subsurface and returns a value that indicates the relative electrical resistance characteristic of the material. Due to the dry conditions of the area of interest, it was likely we would encounter low contact resistance. In order to improve this, a salt water solution was applied to an electrode (see all contact resistance measurements for this study in Appendix 1). The salt water solution had a mixing ratio of 147.4 grams of salt per 3.78L of water (or 1x 26oz. can of salt added to a 5-gallon water jug / backpack sprayer). Prior to data collection for each array, contact resistance was measured. In each instance the contact resistance yielded higher than desired values thus, every electrode in this study was saturated with a salt water solution to improve the contact resistance. Refer to Appendix 1 for all contact resistance measurements that were used in the final collection of data for this study.

There are multiple styles of arrays that are conducted in different fashions based on what the desired outcomes are. In basic terms, most arrays employ four electrodes at once: two current electrodes that transmit (inject) the current (I) into the ground, and two electrodes that measure the potential (V). The distance between electrodes, how they are moved during iterations, transmitter vs. receiver separation, and the symmetry or lack of symmetry are the main differences between array variations. Discussed briefly will be five of the more commonly used arrays. (1)The Wenner array, (2)Schlumberger array, (3)pole-dipole array, (4)dipole-dipole

array, and (5)strong gradient array (Figure 3-2). The Wenner array has been used for one-dimensional vertical soundings. An advantage of using this array is the high signal strength but has a disadvantage of low efficiency in data acquisition, due to single channel utilization (Cubbage, Noonan, & Rucker, 2017), in addition to being very labor intensive as all electrodes need to be displaced and repositioned for each iteration.

In the Schlumberger array, the four electrodes are placed in a line, centered on a midpoint, with the receiving dipole $1/10^{th}$ the separation of the transmitters. The two exterior electrodes inject the current and the two interior electrodes measure the potential. The midpoint remains the same whereas the injecting current electrodes are displaced for further iterations. (Ojo & Olorunfemi, 2018).

Dipole to dipole is one of the more commonly used arrays given the advent of more sophisticated inversion modeling. Resistivity data is plotted at the midpoint between the two dipole, basically providing an intersection data point. The data are then contoured for a representative illustration of the subsurface while inversion software calculates the resistivity values to create an inversion model (Edwards, 1977). Dipole to Dipole has become the standard high-resolution array utilized for resistivity analysis.

The Pole-Dipole array is similar to the Schlumberger in design and employment except for that a receiver is moved outside the transmitter dipole and beyond (displaced up to and beyond 5-10 times the size of the survey area for consecutive iterations). Pole-dipole arrays have far less depth penetration than the dipole to dipole array (Barker, 1989).

The gradient array is a variation of the Schlumberger array. The gradient array is used to measure the potential using a dipole between two fixed current electrodes. The gradient array is best used with a multichannel resistivity system to take simultaneous measurements with the

different potential electrode pairs at different locations (AGI, 2009). The Strong Gradient array is a subset of the Gradient array and imposes that the receiver dipole is $1/10^{th}$ the separation of the transmitter dipole (similar to the Schlumberger array) (Aizebeokhai, & Oyeyemi (2014).

Considering the previously discussed array designs available, this study defaulted to a 2004 study which concluded that dipole-dipole strong gradient array has the best resolution at depth (Stummer, et al., 2004). The array design used was a combination of dipole-dipole and strong gradient, which is referred to by AGI as the Total Field Array. This would give us the outcome of desired depth with desired resolution.

The more electrodes in a survey and the greater the distance between electrodes will yield a wider and deeper inversion model. Although 3-dimensional (length – depth – width) analysis is possible using ERT, only 2-dimensional (length – depth) analysis was utilized. We connected the AGI Supersting™ to the switch box which connected the electrode land cables to electrodes at 10m intervals to measure and record all resistivity measurement. The longer the spacing between electrodes the greater depth potential for analysis; 10m spaced electrodes is the greatest distance available for this study. The Supersting™ was employed at its greatest length potential, 560m long with 56 electrodes spaced 10m apart. The Supersting™ was positioned in the center of the four lines for each execution of an array while executing a roll-along approach (moving the first 25% of the array, or first line from the beginning to the end) multiple times, using the dipole-dipole / strong gradient array.

Two surveys were planned and designed to accomplish the research goals (see Appendix 2 for precise UTM coordinates for both survey locations). Survey A was to provide subsurface information to confirm findings from previous studies for the best location for an alternate well (Karst and Rice, 2018). The second survey, Survey B, was to provide subsurface characteristics

in the vicinity of the inferred fault zone near the boundary to the Pinto Basin. Wilderness and topographic constraints limited equipment transportation and setup; thus, the investigation was confined to the local wash when setting up Survey B. Total ERT survey length for Survey A & Survey B totaled 840m and 960m, respectively. (Figure 3-4).

Before resourcing and setup, an understanding of how deep of an investigation desired was needed to be known. AGI estimates that best depth with resolution can be determined from 20% of the total length of the array (AGI, 2018). Ultimately, the design should be tailored to be able to see to the deepest part of the basin. The USGS estimated with seismic refraction data that depth to bedrock for the entirety of the Cottonwood sub-basin was greatest at 274m bgs (Figure 3-5). From Figure 3-5, it is clear that LUB-23 was drilled in one of the shallower areas of the surveyed line. Despite penetrating approximately 75m of saturated layers, a secondary well could be located at the deepest part of the basin that would penetrate into an area with ~150m of saturated thickness. This could potentially limit vulnerability due to recharge fluctuations in the future. Therefore, the ERT survey design is to attempt to validate the seismic refraction findings. For Survey A, 274m was the target depth which would result in a 1.3km array length. Although this was the intended length, time constraints and topography limited array length to 840m but did include part of the interpreted deepest part of the basin. With the estimated range of depth to water at LUB-23 being between 52-67m (170-219ft), the array design would be able to confirm the recommendation for secondary well siting provided by the NPS in 2018 (Karst & Rice, 2018).

For Survey B, gravity data suggests that the valley fill depth is but a fraction of the area of Survey A at an estimated 25m bgs (Figure 2-4) (Langenheim, et al., 2016). Thus, Survey B was designed at a minimum length of 125m, but was executed at 960m. This extension was

designed in the interest of confirming or denying the presence of fault-like characteristics that could suggest the presence, or lack thereof, a fault-controlled spillway into the Pinto Basin or a groundwater connection between the basins. Survey A consisted of two roll-alongs, or three total array executions, totaling a length of 840 meters and Survey B consisted of three roll-alongs or four total array executions, totaling a length of 980 meters; see Figure 3-6 for a conceptual illustration of this process and Figure 3-4 for survey paths employed. Tomography in this study is used to illustrate the interpretation of collected data from the ER, and the associated EarthImager 2D software from AGI was used to render resistivity inversion to provide ERT for the area of interest (AGI, 2009).

Survey A originated approximately 265m north of the current Cottonwood sub-basin well in the Smoke Tree Wash. The resistivity electrodes were run south along the graded but unimproved road. The entirety of the line was oriented in a north to south direction. A galvanized metal subsurface pipe acted as the transmission line from the well to the treatment and storage infrastructure to the south. This subsurface pipe could introduce uncertainty and is discussed later in the data interpretation. A solar panel farm measuring approximately $11m^2$ is adjacent to the well as the primary power source. A generator house provides the original power to the well but now acts as a contingency power source. A spigot for unknown purposes or design was installed when LUB-23 was installed in 1958. According to park service personnel, this spigot has been leaking for decades and has created a continually recharged pool measuring $1m^2$ in vicinity of the ERT line. This is only mentioned in this study as it was believed it may interfere with ERT results. All electrodes were saturated with the salt water solution to improve contact resistance.

Survey B took place mostly in a runoff wash with less than 10m of relief. The last 190m of a total length of 980 was outside of the Smoke Tree Wash in order to maintain the integrity of a southwest to northeast orientation at an approximate azimuth of 75° magnetic. The same procedure to saturate in immediate proximity of the electrode was used for all electrodes in Survey B. A higher average Ωm contact resistance test vs. Survey A prompted an attempt to improve contact resistance in the wash in the investigation was taking place in. In this instance a shallow cavity was dug, lined with aluminum foil, replaced & saturated the soil, and then drove the electrode through this concentrated solution pocket. This in effect would limit the percolation of the saturation solution and attempt to improve contact with the ground. The resulting contact resistance test yielded no appreciable improvement; therefore, saturation by itself remained the only application to improve contact resistance.

3.2 ERT inversion methodology & data interpretation

ERT collects data through electrical resistivity methods, and the associated inversion provides an illustration or tomographic perspective. Thus, the overall practice and employment is considered Electrical Resistivity Tomography (ERT). The interpretation of data is accomplished through inversion with the subsurface resistivity distribution as the model parameter.

The electrical resistivity methodology described indicates how the difference between the initial injected current and its potential difference (voltage) between two electrodes was measured. The goal of inversion is a map (tomography) from raw data to modeling. Inversion reconstructs the subsurface resistivity distribution from the raw data by mapping from data space to model space from measured voltage and current data (AGI, 2009).

Utilizing EarthImager 2D software from AGI, there are numerous settings and options that can be employed to create a subsurface resistivity distribution. The following is a quick

summary of the main parameters and settings used with the inversion software, specifically the parameters changed from default settings. The continuous Resistivity Profiler (CRP) module is recommended for roll-along ERT surveys, in order to best converge aggregate data versus a singular collection domain (AGI, 2009). Overall, most default settings were maintained but in the initial settings spikes in data were removed along with negative resistivity measurements. Spike data is considered an isolated anomaly in an array within the apparent resistivity. With thousands of data points, a particular area of the subsurface has dozens of iterations interpreting that particular spot. If all but one of the data points measures the same or approximate resistivity, that one anomaly would be considered a spike. Spike data therefore is easily identifiable and likely not accurate. EarthImager 2D removes this spike data (if that option is selected) when running the inverse model, or automatic calibration, of the data. Negative values are common in ERT, and are usually encountered when there are subsurface metallic objects. Despite removing negative values, the presence of subsurface metallic objects can still interfere with the overall interpretation of resistivity data. We altered the smoothness and dampening factors from the default 10 to a value of 100. The smoothness and dampening factors can be interpreted as LaGrange multipliers that balance misfit data and model constraints. When noisy data is expected, a larger multiplier should be used in order to interpret a smoother result. The dampening factor can range from 0 to 10000 and AGI recommends a smoothness and dampening factor of 10 for surface data collection, and a value of 100 for ERT data (AGI, 2009). These two factors balance data misfit and when noisy data is expected it helps for a smooth convergence of data for a more accurate result. Ultimately, all the data should converge, similar to an iterative solver. According to AGI, for ERT, 10-15 iterations should be run for data to converge and to avoid infinite loops so the number of iterations was set to 15 (AGI, 2009). The inversion

modeling for this study never exceeded four iterations to achieve a smooth convergence of data, contributing to confidence in the collected data and subsequent modeling. The accuracy of the resulting profile can be gaged by acknowledging the Root Mean Squared (RMS) error value and L2 values for data misfit. RMS does not indicate the percentage of number of bad points but rather an average data misfit over all of the measurements, thus representative of the quality of fit between the model and the actual measured values. L2 is a measure of data misfit, and refers more to the convergence of the data, reflecting unity of the data with the profile. When the L2 value is 1.0 or less, the inversion is considered converged. However, it is recommended that the data inversion is more dependent on the RMS value rather than L2. Focusing on data convergence (checking the option for L2-Norm) could result in neglecting to consider the reduction of the RMS value, and focus on L2. Ultimately, for an accurate profile the goal is a balance of an RMS value below 5% and an L2 value close to or less than 1. With these values it ultimately means that the true model varies relatively little from the inversion model.

The data inversion modeling as discussed will yield a profile of ohm-m contours. The color palette chosen for the profiles are red to blue with decreasing resistivity respectively. Solid red would suggest high resistivity and dark blue would suggest low resistivity. For the purposes of this research we will interpret that any resistivity measurements between 3-100 Ωm could be moist substrates that include clayey, wet clay, silty soils and clay, sandy soils and gravels (Burger et al., 2006). Resistivity measurements beyond 100Ωm can include any number of geologic circumstances and each observation that could prove a circumstance likely has an exception. The scope of this research is to identify wet to moist layers if possible and contribute to the body of knowledge for understanding the subsurface, but will not be identifying the subsurface geology as resistivity ranges for geologic materials are very non-specific (Table 3-1).

3.3 Geochemical Collection & Processing Methodology

Well water temperature, pH, specific conductance, alkalinity, dissolved oxygen, general chemistry, and stable isotope composition were determined using water samples collected from LUB-23 pre-treatment. The source for collecting the groundwater, was a spigot that was connected directly to the well transmission line that was housed inside the generator house.

Two Oakton multi-parameter PC Testr 35 probes were used to measure water temperature, pH, and conductance in order to provide dual-source confidence. Both were calibrated the day of measuring. An Extech DO600 ExStik II dissolved oxygen (DO) meter was used to measure DO and was calibrated the same day of measuring with elevation calibration considerations (900m / 2953 ft above sea level). Hach method 8203 was followed to determine alkalinity of the water whereas general chemistry and stable isotopes values of LUB-23 groundwater were requisitioned from Test America Labs, Irvine, CA.

In order to ensure as much air has been removed from the sample line as possible, the spigot was turned on and remained on for several minutes until a continuous and smooth flow was evident. A brass adapter was used to connect the spigot to PVC tubing in order to facilitate efficient means of collection. Two 500 mL Nalgene bottles were filled with sample water and allowed to settle to ensure no air bubbles were present. After 5 minutes, approximately 150 mL were poured from each bottle into two separate glass beakers that could accommodate the probes to measure. The same methodology was used to collect sample water to measure dissolved oxygen. Several samples were collected for general chemistry in accordance with the Test America sampling and packing protocol. All samples for requisitioned analysis were packed on ice and sent the same day via commercial courier to Test America. All samples in this study were compared to water quality analysis from samples taken in 2009 from LUB-23. The stable

isotopes compared were Deuterium (δ^2H) and $\delta^{18}O$. Chemicals sampled included cations, anions, some metals with general chemistry measuring the total dissolved solids and alkalinity.

3.4 Well observation data methodology

Two tools were available to determine depth to water in LUB-23, as well as to attempt to assess the condition of the well. First was a 500 ft WL500 well sounder and second used was a digital camera attached to a power and optics line small enough to navigate through the well cap. The well sounder and camera were used in tandem to confirm observations and provide a high level of confidence for data acquired.

Table 3-1. Common materials and their respective resistivity found using ERT. Source credit: AGI, 2008.

Material Type	Resitivity Range (Ωm)	
	Low	High
Igneous	100	1000000
Limestone	100	10000
Sandstone	100	1000
Sand & gravel	600	10000
Clay	10	100
Unconsolidated wet clay	20	
Soil	1	10
Fresh Water	3	100
Drill mud, hydraul-EZ	4.5	
Sea water	0.2	1
Copper	0.0000002	

Figure 3-1a. Equipment Layout. (A) ERT Switch Box, (B) ERT Supersting™ R8, (C) 2x Deep Cycle Marine Batteries, (D) 4x ERT Electrode (10m spacing) Land Cables.

Figure 3-1b. An electrode connected to the electrode land cable.

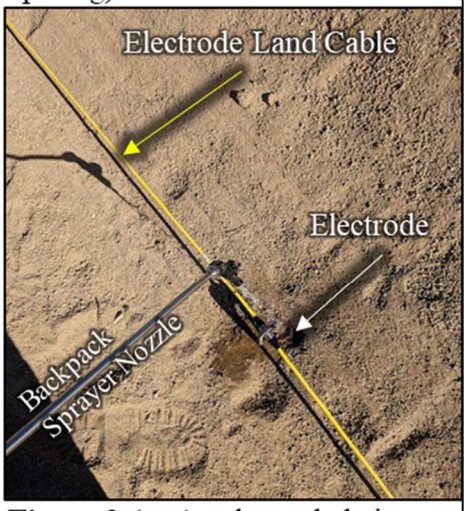

Figure 3-1c. An electrode being saturated with a salt water solution.

Figure 3-1. AGI SuperstingTM Equipment. Layout to include associated peripherals.

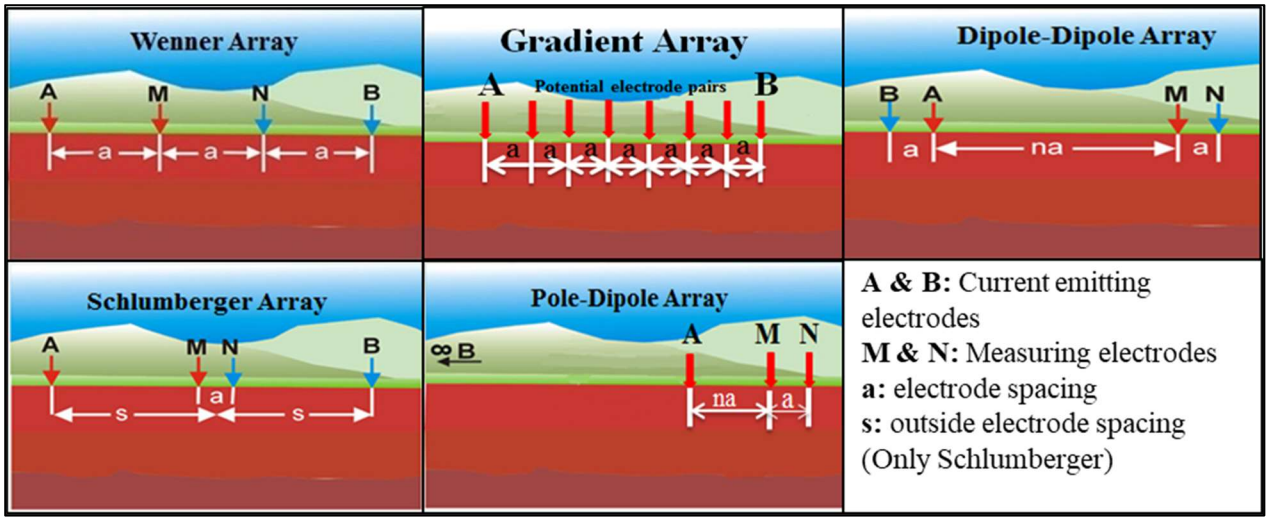

Figure 3-2. ERT Array Orientation. A visual illustration of varying electrical resistivity array designs. Source credit: AGI, 2017 (https://www.agiusa.com/blog/comparison-11-classical-electrode-arrays)

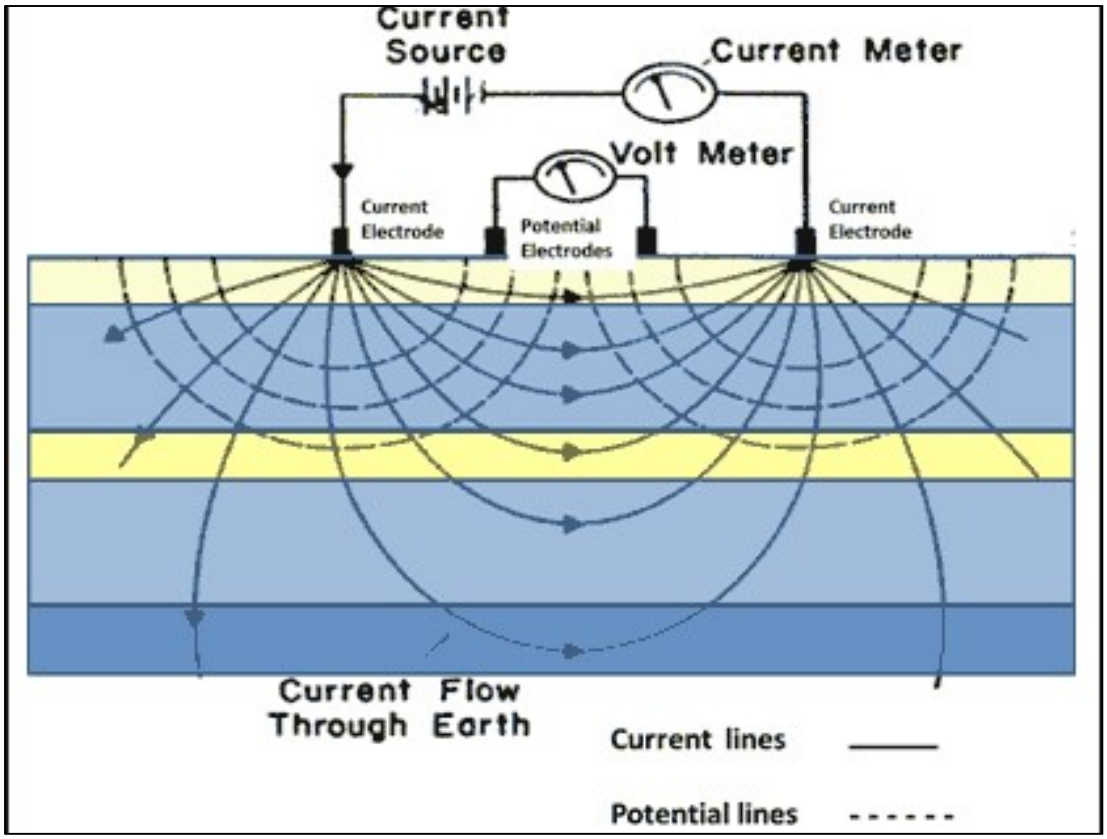

Figure 3-3. Conceptual illustration of Employing an ERT Array. Source credit: P. Chandra http://www.aquiferindia.org/Surface_Geophysical_Methods.aspx

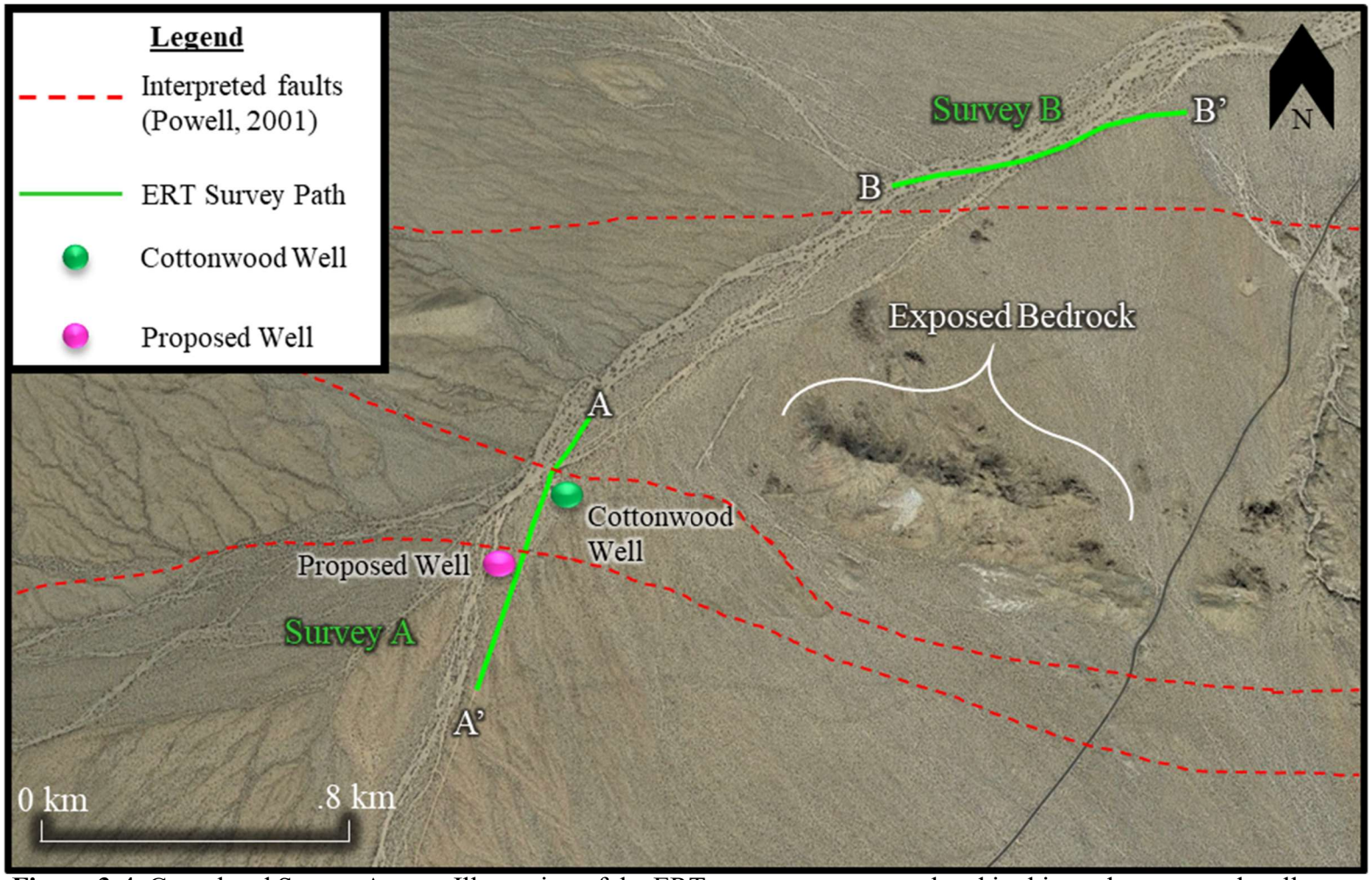

Figure 3-4. Completed Survey Arrays. Illustration of the ERT survey arrays completed in this study, proposed well location, and local Smoke Tree Wash faulting as interpreted from Powell, 2001.

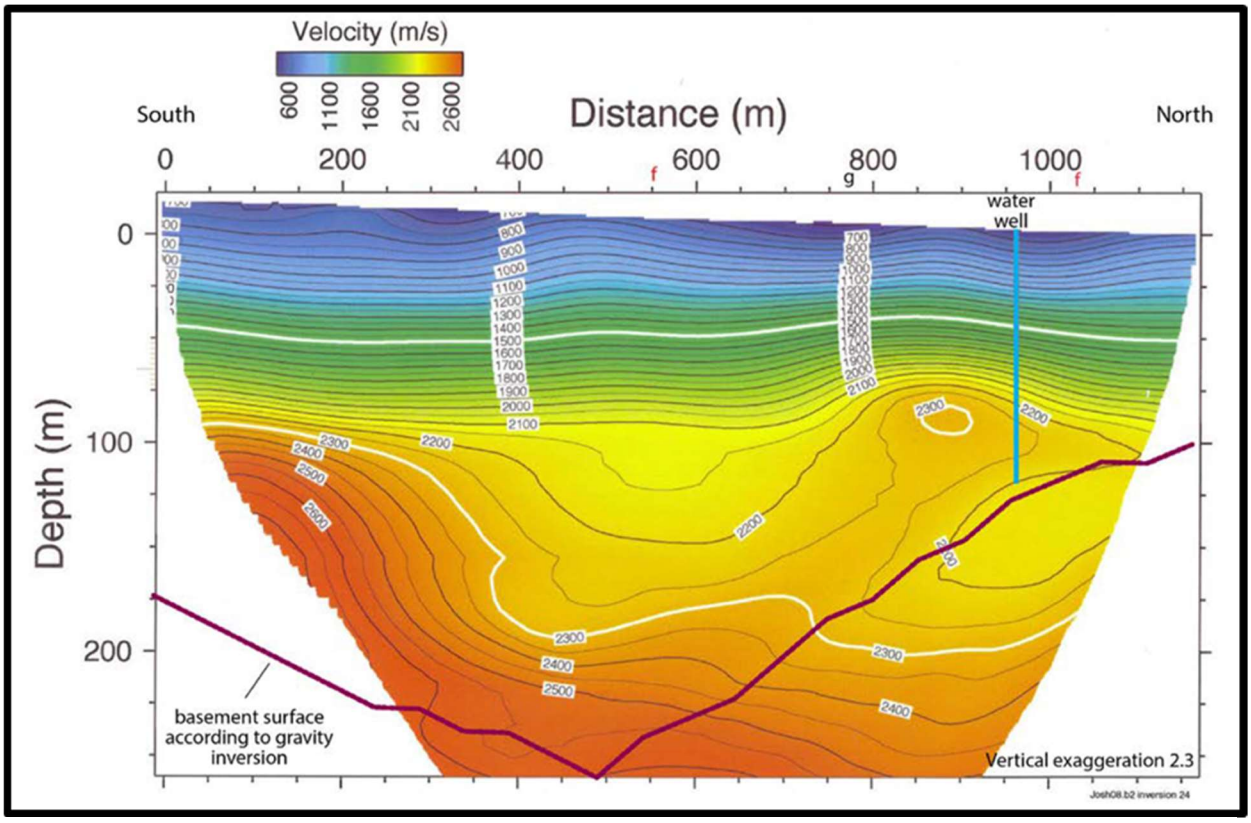

Figure 3-5. Seismic refraction data. Cottonwood sub-basin with LUB-23 labeled, primarily along the unimproved road and extending ~250m beyond. Source credit: Langenheim, et al., 2016.

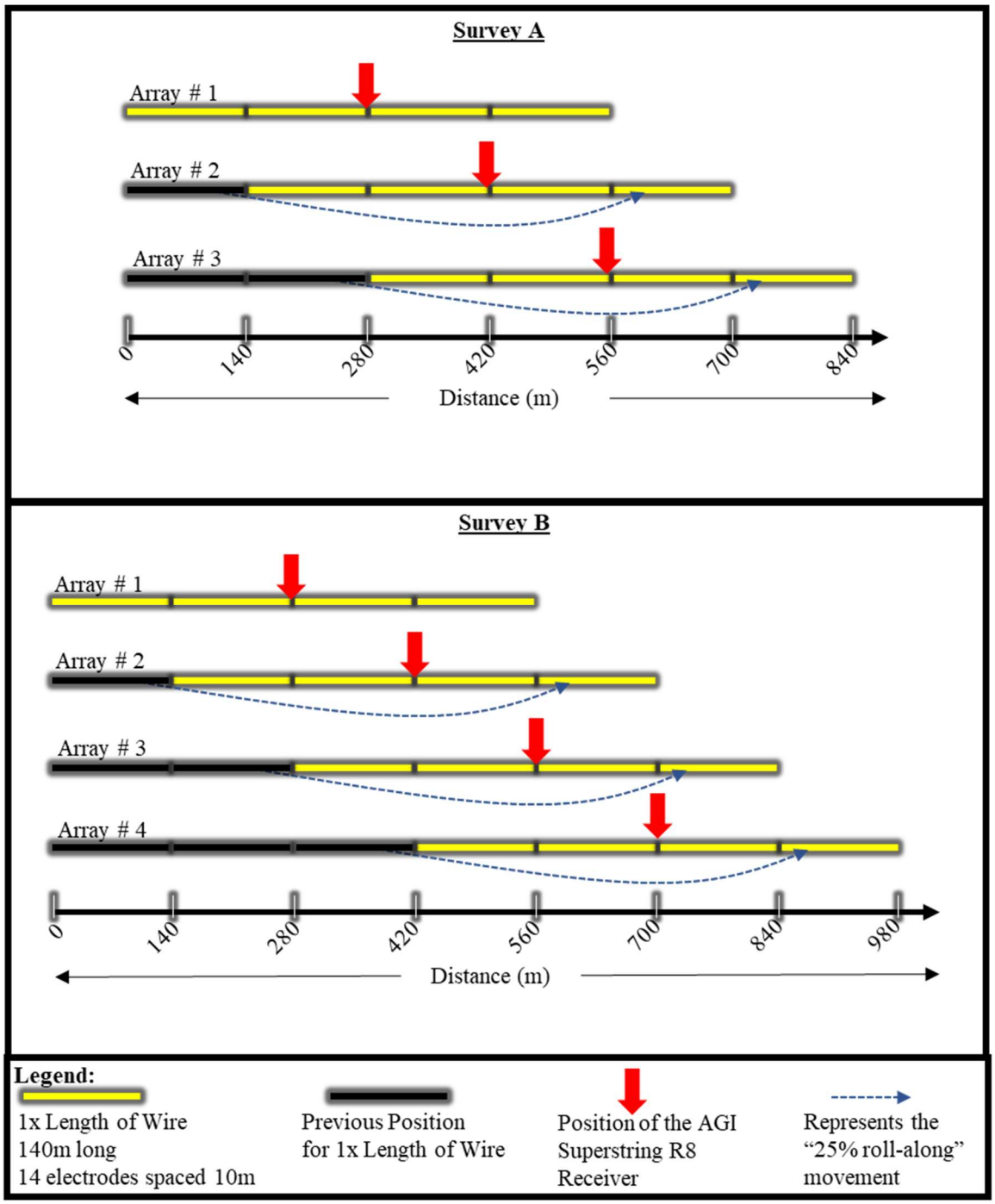

Figure 3-6. ERT Roll-Along Conceptual Illustration. Both survey approaches in this study are illustrated.

4. RESULTS

The results of ERT inversion modeling using Earthimager 2D software show a contoured interpretation of the associated resistivity distribution of the subsurface. In this section we will describe the resistivity model and how it changes by location. Particularly, we will describe certain zones that are relevant to understanding how water could flow in the Cottonwood sub-basin and how it relates to the investigation and overall study.

4.1 ERT Results: Survey A.

Survey A was 840m in total with 600m along a graded but unimproved road and 240m in a wash north of LUB-23 (Figure 3-4). Considerations that may have affected results for this survey include a solar panel farm with associated subsurface electrical infrastructure in proximity to the well, the subsurface well water transmission line, and a continually dripping spigot that leaks water from LUB-23 (Figure 4-1). Lack of records from when the well was installed do not show where this transmission line. It is currently assumed by park personnel that a galvanized metal pipe is in the area between the well (LUB-23) and the generator house, then proceeds south toward the visitor center infrastructure on the western-most side of the road (referred to as "Path of Survey A" in Figure 4-1).

A contact resistance test was performed before collecting any data and again after each roll-along (Figure 3-6). The values in Survey A for contact resistance range from approximately 425 - 3,300 Ωm. These values are very good for the environment being employed, as it falls within the threshold of reliable contact resistance readings according to AGI (AGI, 2009). As previously described, the application of a salt water solution provided the best possible contact resistance given the climate and surface conditions.

Figure 4-2 represents the data misfit histogram for collected data in Survey A. Survey A analyzed a total of 2,069 data points. Each data point is a measurement of resistivity at a certain location based on the dipole-dipole strong gradient array approach. Of these 2,069 data points, 61 points (2.9%) of data was excluded from the analysis as removal of these values returned the best RMS and L2 combination for model accuracy. The process to determine what data were to be removed was trial and error. Several iterations of running the data selecting different data to exclude were run to determine which complete data set yielded the lowest RMS with an L2 close to 1. This process also included a model with all data with no removal or spikes, negative values, or noisy data. Ultimately, removing 61 data points as illustrated in Figure 4-2 provided a model resulting in a data misfit cross-plot Figure 4-3. The RMS of this array was 2.58% with an L2 of 0.73, meeting the threshold of having relatively minimized error and well converged data.

Figure 4-4 represents the resistivity contours of the subsurface for Survey A inversion. Figure 4-5 is the same figure as 4-4 but with added location identifiers to aid in referring to specific sections. Refer to Figure 4-5 for the following observations. Location (A) is a saturated area with a resistivity less than 40Ωm, with consistent depth as it progresses longitudinally, but only remains consistent when data is collected in the wash. This layer averages a thickness of 13.5m and starts at a depth bgs of 13.5m and extends to 27m bgs. This low resistivity layer is absent when the survey transitions from the wash to the road. Location (B) has the highest resistivity in the area at 150 Ωm, and remains consistently parallel to the wash at a depth approximately 41m bgs. Location (C) is a very low resistivity area approximately 27m thick starting at a depth ~13.5m below ground surface and has a longitudinal width of approximately 40m. Location (D) is a relatively contiguous high resistivity area between 60-150Ωm, overlapping the border between the wash and the road. This location consists of two high

resistivity areas (both at ~150 Ωm) connected by a moderately resistant layer (relative to the area) at ~60Ωm. This area also suggests the presence of a fault. Consistent with Powell's interpretation of faults in the area as well as the clear sediment change and angled orientation consistent with a fault caused by extension in a pull-apart basin. Location (E) are relatively uniform fluctuations or oscillations in resistivity measurements nearly identical to electrode locations at shallow depth (less than 5m). These fluctuations occur in the road area directly above what has been referred to as the deepest part of the basin (between 330m-430m longitudinally from the start of Survey A). Location (F) is a large low resistivity area less than 35 Ωm at 400m into the survey, located underneath the road with an observed thickness of at least 50m thick. Location (G) is a relatively uniform low resistivity area (less than 80Ωm throughout).

4.2 ERT Results: Survey B.

A contact resistance test was performed before collecting any data for Survey B and again after each roll-along as described in Figure 3-6. To reiterate, all electrodes for all surveys were saturated with salt water solution to help improve this contact resistance. The range of contact resistance in Survey B ranged from 1000 Ωm through 7500Ωm with the average ranging from 2500-3200 Ωm; which is considered usable and accurate. With higher contact resistance readings, we expected to have a larger abundance of noisy or spike data. However, being in wilderness with no anthropogenic influences (like Survey A) this expectation was relatively offset to return minimal data that was excluded from modeling. In the arid environment of collection, the collected contact resistances were within the threshold of useable and reliable. According to AGI, any data collected that has a contact resistance of greater than 10,000Ωm should be dismissed as a poorly installed electrode (AGI, 2009). Ideally, an adequate contact resistance is less than 5,000Ωm. The highest contact resistance we had for Survey B was 7,500

Ωm with the majority of measurements falling between 2,500 and 3,200 Ωm. Approximately 5% of data had a contact resistance greater than 5,000 Ωm and less than 1% was greater than 6,500 Ωm. This summary of contact resistance values was better than expected (even when using the salt water solution) and provides usable and accurate data

Figure 4-6 represents the data misfit histogram and Figure 4-7 represents the data misfit cross-plot for collected data in Survey B. Survey B collected 2,524 data points. The same trial and error approach was used similar to the data misfit removal of bad data for Survey A. Of the collected 2,524 data points, 165 points (6.5%) were omitted as bad values. The RMS of 2.7% and L2 of 0.81 reflects quality data with good convergence.

Figure 4-8 presents the inverted resistivity contours for Survey B. Figure 4-9 is the same figure as 4-8 but with added location identifiers to aid in referring to specific sections. Refer to Figure 4-9 for the following observations. Location (A) is a very low resistivity layer with a resistivity measuring less than 50 Ωm. It has an average thickness between 7-10m at an average shallow depth between 10m - 13.5m bgs. This low resistivity area exists parallel to a high (relative) resistivity layer beneath it (between 100-408 Ωm). This layer persists from the start of the survey for approximately 700m beneath the Smoke Tree Wash until the higher resistivity layer beneath it is absent. Location (B) is a high (relative) resistivity layer ranging between 100-408Ωm with the majority of the area having a resistivity measure greater than 300Ωm. Location (C) is an area of low resistivity (less than 100Ωm) bridging between two relatively higher resistivity areas. This low resistivity layer is uniform in resistivity from the surface to a depth of at least 109m bgs and is approximately 110m in longitudinal width. Location (D) is a higher resistivity area on average with an approximate measure of ~125Ωm and is located outside of the

wash. Location (E) is representative of uniform fluctuations or oscillations in readings near the surface correlating to electrode locations.

4.3 Geochemical Results

Table 4-1 outlines the water quality analysis from 2009 samples and the resulting values from this study in 2018 respectively. Two Oakton meters were used in order to validate the respective, providing confidence in measurements. These meters were used to measure temperate, pH, conductivity, and dissolved oxygen with only minor variations between the two different meters. Test America Labs was responsible for the water quality analysis as indicated in Table 4-1 measuring metals, anions, and general chemistry; a full list of methods and results is located in Appendix 4.

4.4 Well Observation Results

Utilizing a snaking camera and well sounder, a visual inspection was conducted on the interior of the well to a total depth of approximately 70m (231 ft) bgs. For clarification, the video investigated to a depth of 71.30m (234 ft), however, the entry into the well casing was .73m (2.4ft) above the ground surface with a total of 71.3m (234ft) of cabling extended from the spool. After taking into consideration the height above ground surface that the camera enters the well casing, we measured a depth to water of 58.5m (190.78 ft) bgs.

Figure 4-10 illustrates a short pump drawdown and recovery test. A 15-minute pump and recovery test was conducted which showed a near instantaneous recovery and drawdown relationship. This behavior suggests the screening of the well is not clogged and is in adequate working order.

Table 4-1. LUB-23 Water Quality & Isotope Analysis (2009 vs 2018)

LUB-23 Water Quality Comparison 2009 vs. 2018		
Water Quality Parameter	**2009**	**2018**
Dissolved Oxygen (mg/L)	7.60	6.44
Water Temperature °C	15	16.7
pH **[F]**	7.7	7.9
Specific Conductance **[F]** (µS/cm)	428	451
Alkalinity **[F]** (mg/L as $CaCO_3$)	120	101 **[H]**
Chloride (mg/L)	40.1	38
Nitrate (mg/L)	1.47	1.5
Fluoride (mg/L)	2.9	2.8
Sulfate (mg/L)	26.9	27
Boron (mg/L)	0.16	0.13
Calcium (mg/L)	36.5	34
Magnesium (mg/L)	6.9	6.7
Potassium (mg/L)	1.75	1.7
Sodium (mg/L)	39.50	37
Aluminum (µg/L)	ND	9.5
Arsenic (µg/L)	2.1	2.2
Barium (µg/L)	43	36
Copper (µg/L)	ND	1.1
Lead (µg/L)	≤ 0.04	ND
Iron (µg/L)	9	ND
Manganese (µg/L)	2	0.83
Uranium (µg/L)	3.46	3
Zinc (µg/L)	237	63
Alkalinity as $CaCO_3$ **[L]** (mg/L)	123	120
Bicarbonate Alkalinity as $CaCO_3$ **[L]** (mg/L)	149	120
δ^2H (‰ relative to VSMOW)	-70.8	-71
$\delta^{18}O$ (‰ relative to VSMOW)	-9.78	-9.8

[F] – Field Measurement
[L] – Lab Measurement
[H] – Hach Method 8203
2009 – Source Credit: Methany et al., 2012
2018 – Outsourced water quality analysis conducted by Test America Labs (Irvine, CA Job ID: 440-225417-1), except where indicated
ND – Not detected

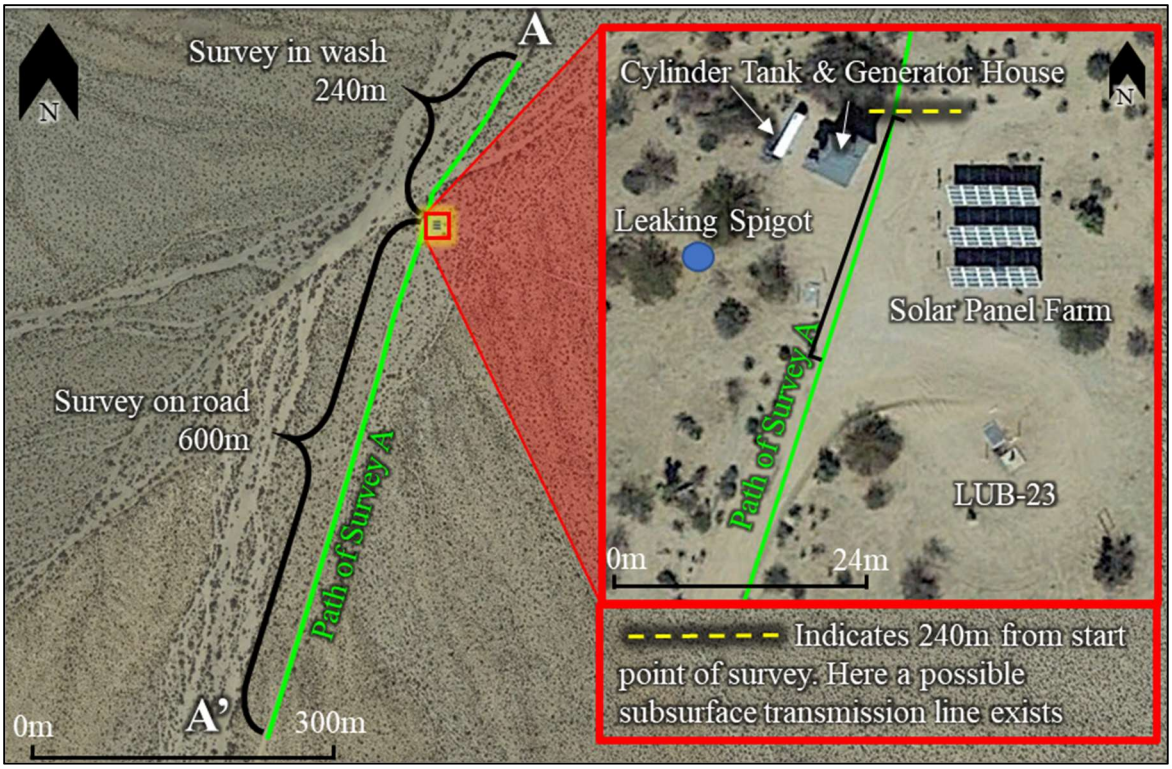

Figure 4-1. LUB-23 Site Orientation.

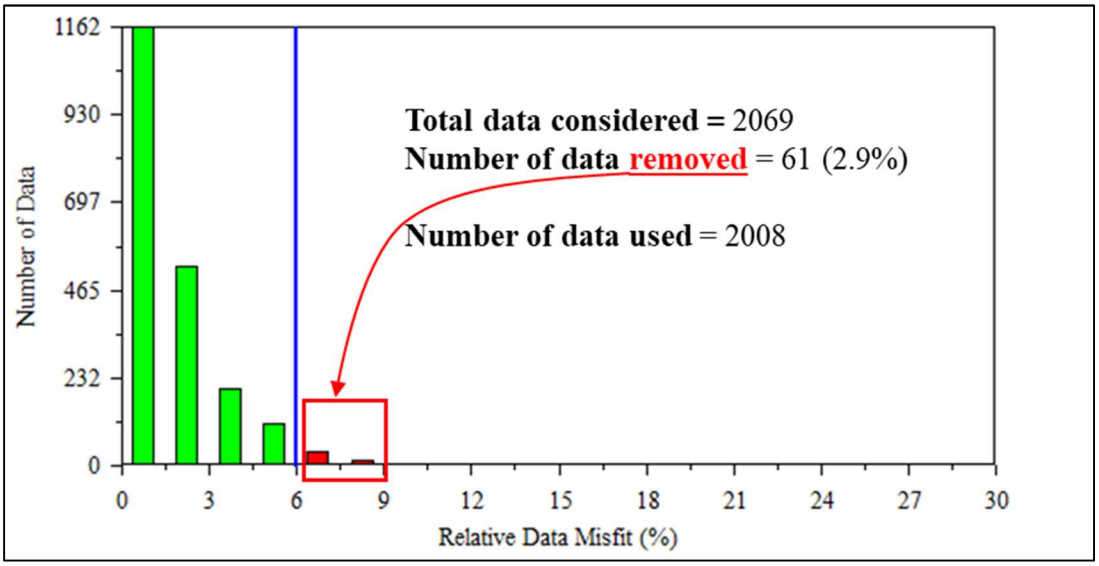

Figure 4-2. Survey A: Data Misfit Histogram.

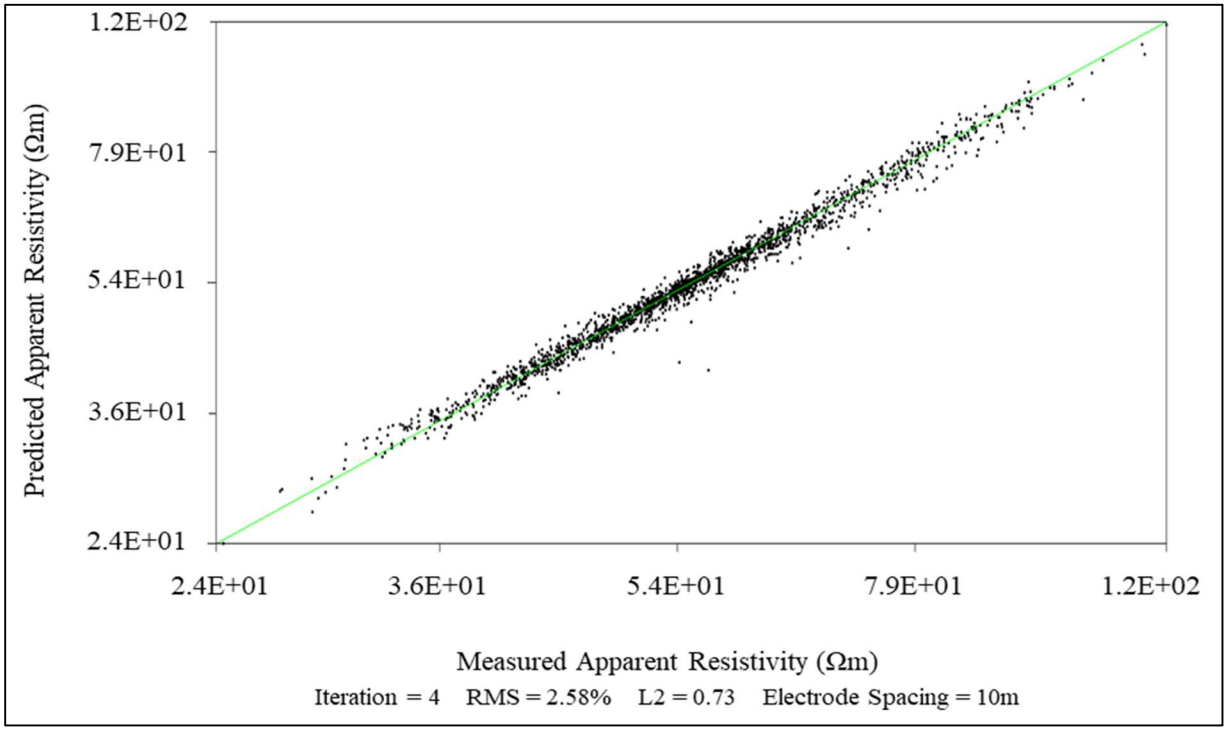

Figure 4-3. Survey A: Data Misfit Cross-Plot. Measured vs. Predicted Resistivity Values.

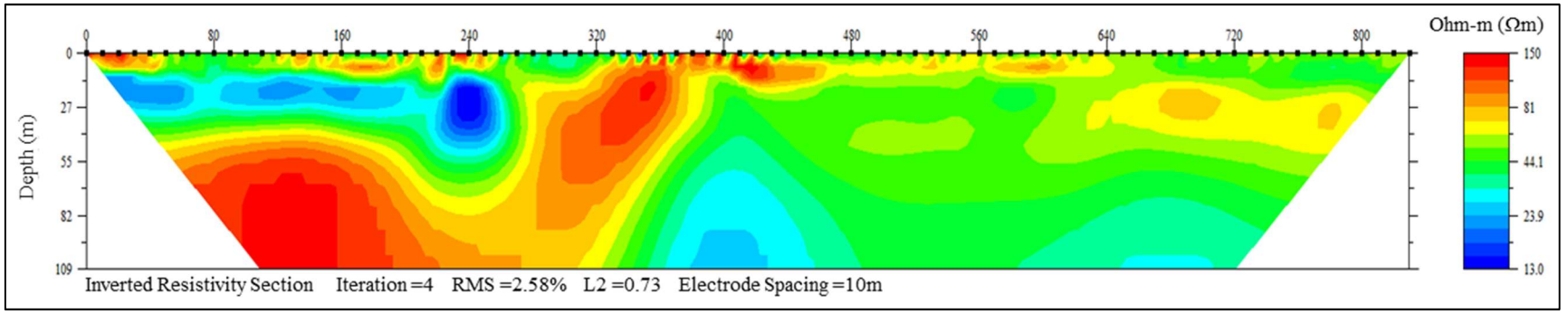

Figure 4-4. Survey A: Unmodified Resistivity Inversion Results

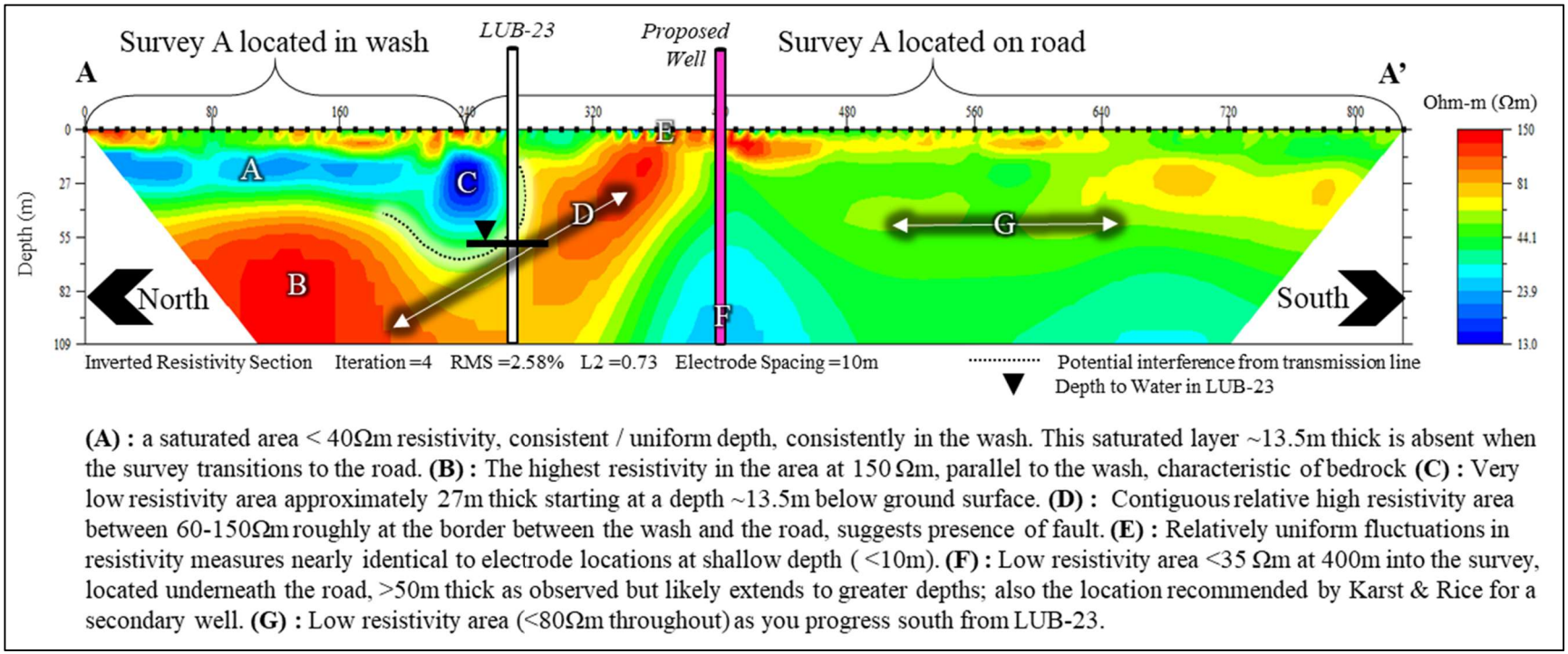

(A) : a saturated area < 40Ωm resistivity, consistent / uniform depth, consistently in the wash. This saturated layer ~13.5m thick is absent when the survey transitions to the road. **(B) :** The highest resistivity in the area at 150 Ωm, parallel to the wash, characteristic of bedrock **(C) :** Very low resistivity area approximately 27m thick starting at a depth ~13.5m below ground surface. **(D) :** Contiguous relative high resistivity area between 60-150Ωm roughly at the border between the wash and the road, suggests presence of fault. **(E) :** Relatively uniform fluctuations in resistivity measures nearly identical to electrode locations at shallow depth (<10m). **(F) :** Low resistivity area <35 Ωm at 400m into the survey, located underneath the road, >50m thick as observed but likely extends to greater depths; also the location recommended by Karst & Rice for a secondary well. **(G) :** Low resistivity area (<80Ωm throughout) as you progress south from LUB-23.

Figure 4-5. Survey A: Interpreted Resistivity Inversion Results

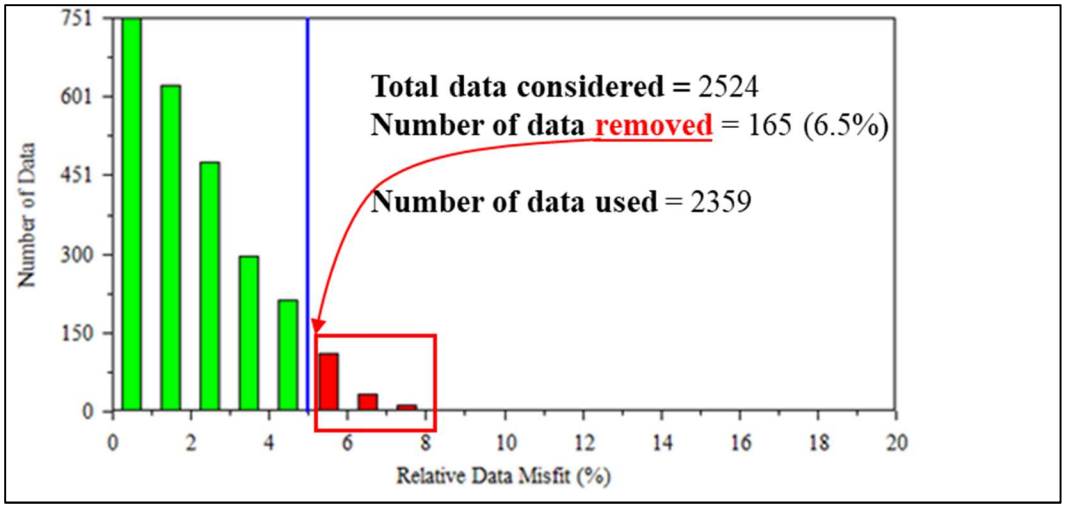

Figure 4-6. Survey "B" data misfit histogram.

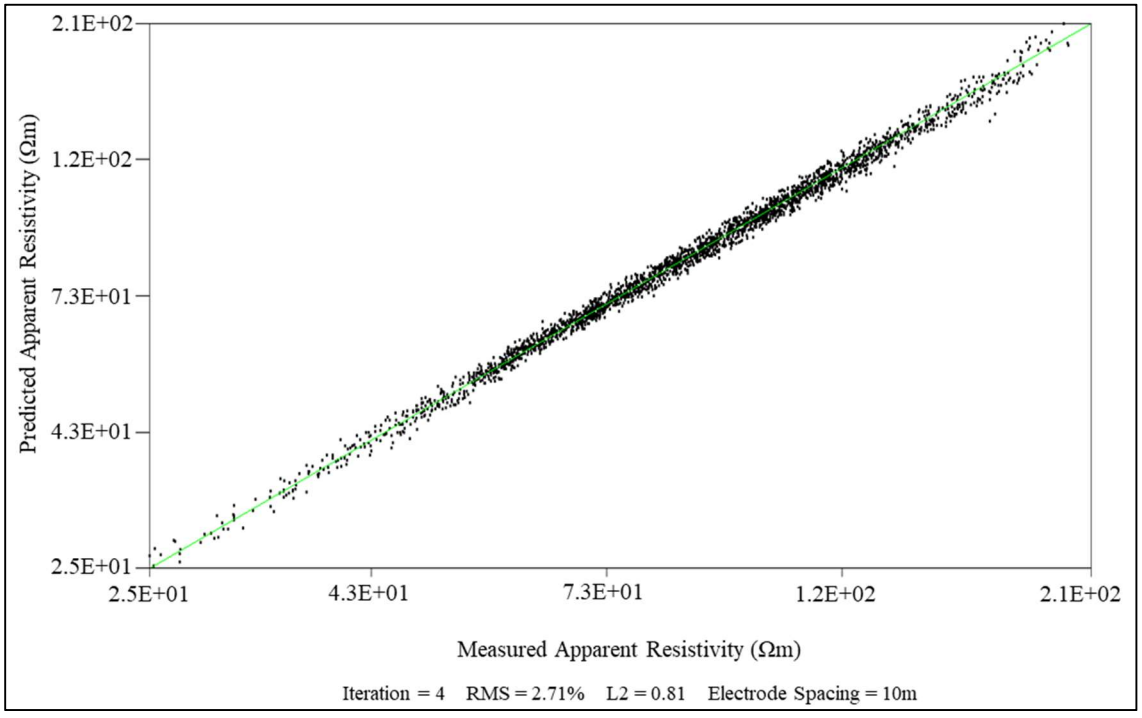

Figure 4-7. Survey B: Data Misfit Cross-Plot. Measured vs. Predicted Resistivity Values.

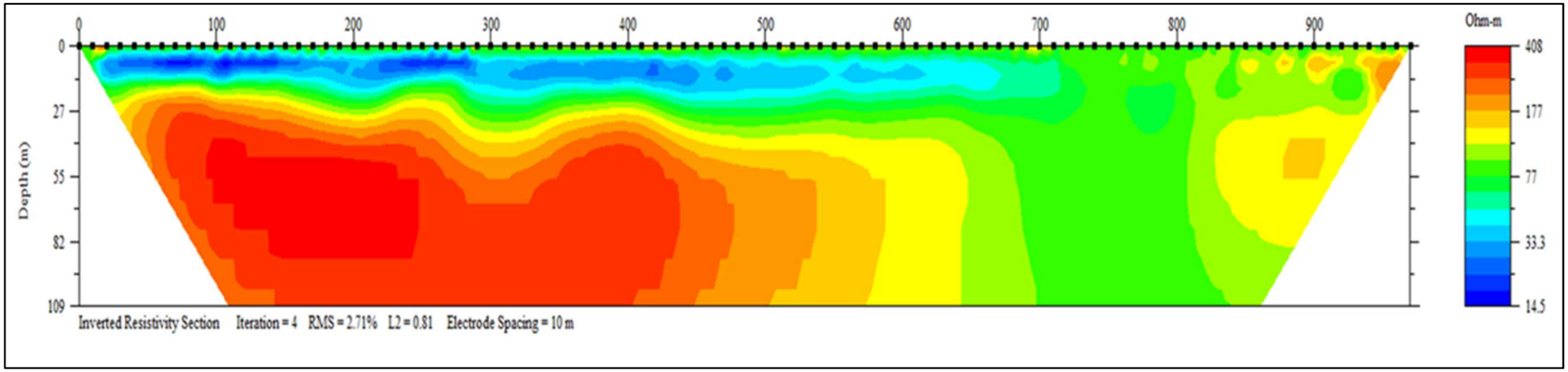

Figure 4-8. Survey B: Unmodified Resistivity Inversion Results.

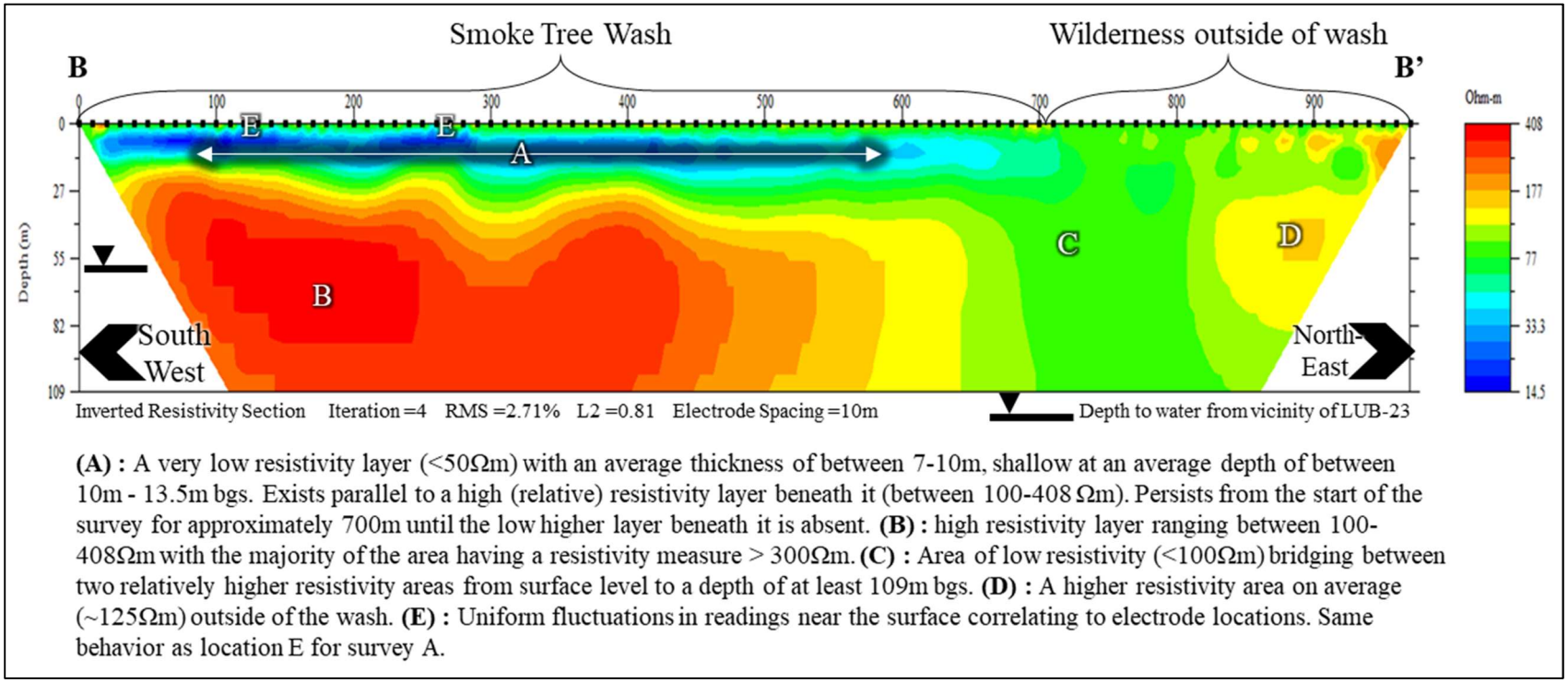

(A) : A very low resistivity layer (<50Ωm) with an average thickness of between 7-10m, shallow at an average depth of between 10m - 13.5m bgs. Exists parallel to a high (relative) resistivity layer beneath it (between 100-408 Ωm). Persists from the start of the survey for approximately 700m until the low higher layer beneath it is absent. **(B) :** high resistivity layer ranging between 100-408Ωm with the majority of the area having a resistivity measure > 300Ωm. **(C) :** Area of low resistivity (<100Ωm) bridging between two relatively higher resistivity areas from surface level to a depth of at least 109m bgs. **(D) :** A higher resistivity area on average (~125Ωm) outside of the wash. **(E) :** Uniform fluctuations in readings near the surface correlating to electrode locations. Same behavior as location E for survey A.

Figure 4-9. Survey B: Interpreted Resistivity Inversion Results.

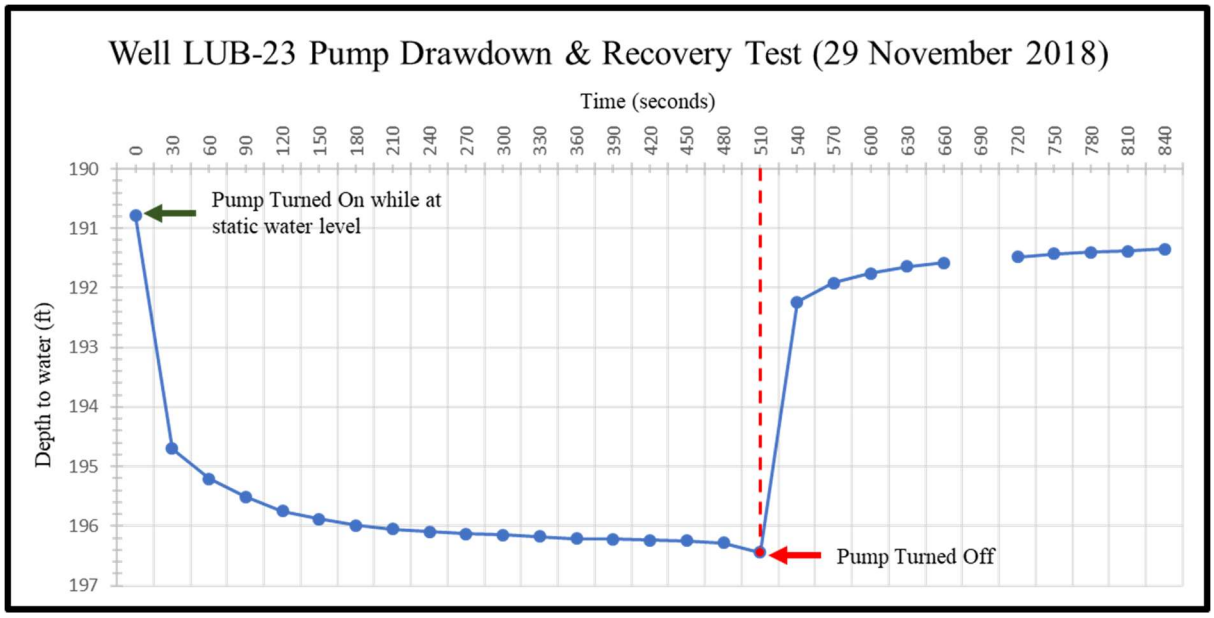

Figure 4-10. LUB-23 Pump Drawdown & Recovery Test. Cottonwood sub-basin, Joshua Tree National Park (29NOV18).

5. DISCUSSION

5.1 ERT Discussion: Survey A

Refer to Figure 4-5 to visualize the following interpretations of data. Location A of Survey A is a wet or saturated layer directly beneath the wash and averages a resistivity measurement of approximately 40Ωm. This layer begins at approximately ~13.5m bgs and averages ~13.5m thick. This layer is likely the result of infiltration from overland flow on 13 October 2018 (6 weeks prior to data collection) which was an event of 60mm (2.34") of precipitation, nearly 33% of all the precipitation that fell in the area in 2018. The existence of this layer is directly correlated (and parallel) to the wash as it ceases to exist when measurements are taken outside of the wash. This could be a result of a more permeable subsurface and the infiltrating waters are able to travel deeper into the subsurface, or more likely, that overland flow is contained within the washes of the area limiting the likelihood for the concentration of subsurface waters outside of the washes. A study in the very arid Gidron Wadi area of Israel observed similar low resistivity areas that were interpreted as perched subsurface water that underlie ephemeral streams (Winters, et al., 2015). With similar climate and aridity to this study area this finding supports the interpretation of this low resistivity layer being a non-persistent underflow. The arid Smoke Tree Wash could be characterized as similar in nature to ephemeral streams substantiating the interpretation of this low resistivity area as saturated.

Location B has the highest relative resistivity in the area (150Ωm). The previously described saturated layer seems to be perched above it. However, it cannot be determined whether the saturated thickness would continue to infiltrate further into this higher resistivity area with this data collection alone. This increase in resistivity could indicate an area of lower permeability or a change in sediment type. The resistivity contour indicates a change to this

higher resistivity layer at a depth of 41m (134 ft). The driller's logs for LUB-23 (Table 2-1) show that at 41m (135ft) bgs, the subsurface transitions from boulders and clay content to sand and clay content. Published works suggest that dry sand and gravel has a resistivity between 600-10,000Ωm but since the subsurface stratigraphy appears to be consistent with respect to transition areas, we can assume that the resistivity of the described young alluvium is either lower than 600Ωm as indicated or the recent precipitation event has altered the inherent resistivity in this area.

Location C (transition point from wash to road), is an extremely low resistivity area and likely the result of an underground transmission line. Measured at 240m from the start of the survey it is close to where LUB-23 is located (270m from the start of the survey). Schematics and record keeping have not been acquirable for LUB-23 with respect to the subsurface infrastructure and transmission. However, the circular shape in the approximate area where it would be expected to be (generator house next to the well), suggests this to be the transmission line. Furthermore, the transmission line is known to be a galvanized metallic pipe and further brings into question the validity of data in this area. Some indications of this is the circular extension of the low resistivity area into the surrounding higher resistivity area, marked by a dashed black line in Figure 4-5. Referencing the driller's logs from Table 2-1 reinforces the probability of interference. The logs note increasing resistivity areas as shallow as 35m (115ft) bgs where we should expect higher resistivity readings based on the lithology differences. However, relatively low and uniform resistivity readings extend to depths of about 60m (196ft) bgs in a spherical and odd shape around the assumed transmission line. The presence of a solar panel farm is also at the 240m (787ft) position from survey start, at the same area of this low resistivity circular area. The solar panels are connected to the subsurface pump in LUB-23 and is

the primary power source. However, the subsurface pump is connected to the generator house as well to be run as a contingency. The subsurface electrical infrastructure is not well recorded for park personnel to access, so it is not known the extent of possible interference in this area. The reliability of data immediately surrounding the possible transmission line and in its immediate proximity is low and should be dismissed from interpretation.

Location D (on road), has relative higher resistivity appears to be a contiguous element extending from the same section as location A. Uncertainty is increased in this assessment due to the questionably lower resistivity in the area immediately under the assumed transmission line.

Location E (near surface, occurring both in wash and on road), shows several fluctuations or oscillations in a general "U" shape extending down from the surface that have a lower resistivity than its surroundings. These areas are uniform in distance and directly correlate to electrode placement. These oscillations are likely attributed to the application of the salt water solution at each electrode every 10m. They may be due to the sharp resistivity gradient around high and low contact resistance and the assumption of low noise in the inversion. Therefore, data interpretation at and immediately below the surface should be disregarded but, data beneath approximately 5m is deemed good (Greenwood, Jason, 2019). These oscillations extend approximately 5m into the subsurface and are also found in Survey B (later discussed).

Location F (on road), suggests a low resistivity zone (34Ωm and less) starts at 370m into the survey and begins at a depth of 60m (196ft) bgs extending to at least 109m (357ft) bgs. It is likely that this is the saturated zone of the basin and the saturated thickness extends to bedrock depth and is connected to the adjacent saturated area at similar depth at 670m from survey start. This saturated area at 400m from the survey start point is the same location where Karst & Rice (2018) recommended a second site for a well to be placed as an alternate or secondary well

(Karst & Rice, 2018). This area has also been determined to be the deepest part of the basin according to seismic refraction data and isostatic gravity data (Langenheim et al., 2016). In terms of available saturated areas along the length of the road capable of joining the existing infrastructure, this study agrees with this alternate location as the best recommendation.

Location G (on road), has a generally low resistivity throughout the subsurface distribution. Localized areas of higher resistivity suggest a change in sediment which is consistent with Weir & Bader's (1963) interpretation of having dispersed areas of clay and lacustrine deposits amongst the younger and older alluvium. Nothing suggests saturation in this area until you reach depths of 100m bgs.

Another observation includes a leaking spigot at approximately 262m from the start point of the survey (Figure 4-1) connected directly to LUB-23. It has been consistently leaking since, what is assumed to be, 1958. A consistent pool approximately $1m^2$ persists year-round, to the point it has created its own small ecosystem. It does not appear to have influenced ERT data nor can we see resistivity evidence to this point but 262m is also at the area of uncertainty from the assumed transmission line.

5.2 ERT Discussion: Survey B

Refer to Figure 4-9 to visualize the following interpretations of data. At Location A of Survey B (within a wash) a relatively shallow layer is observed with a resistivity value averaging between 14.5Ωm and 55Ωm. At a depth bgs ranging from 5m bgs to 15m bgs this layer has thickness of approximately 13.5m. This layer extends nearly 700m or the longitudinal distance of the array that was surveyed in the wash. The existence of this layer is directly correlated (and parallel) to the wash as it ceases to exist when measurements are taken outside of the wash. The

likely interpretation for this layer is overland flow is contained within the washes of the area limiting infiltration to the subsurface outside of the washes.

Location B (in wash), a high resistivity area with an average resistivity between 177Ωm and 408Ωm. In this location the high resistivity area starts at a shallower depth around 27m bgs but extends to at least 109m bgs. Isostatic gravity data are consistent with the ERT findings as this area of the Cottonwood sub-basin is interpreted as shallow respective to the valley fill depth (Langenheim et al., 2016). The area surveyed is placed along the peripheries of the Cottonwood sub-basin and the Pinto Basin in order to help refine the hydrogeologic relationship between the two basins. Bedrock for this area is defined as granite or metamorphic rock which would have a resitivity at least 2-3 orders of magnitude greater than collected data. This resistivity measurement averaging at 500Ωm is consistent with consolidated sand and gravel units.

Location C (mostly out of wash), has a moderate (relative) resistivity layer starting at 670m from the start of the survey to 800m from the start. A consistent resistivity measurement of 77Ωm begins at ground surface and extends to at least 109m below ground surface which suggests unconsolidated younger alluvial deposits but are not wet or saturated. This uniformity and clear divide between stratigraphic areas could indicate a fault, particularly since this survey is in an inferred fault zone. The near vertical interpretation of this resistivity area suggests that it is not, as we would expect to see a normal fault from extension with a hanging and foot wall similar to Figure 1-5. If a fault, it could also imply that B→D are one unit that has been divided by C.

Location D (out of wash), shows a higher resistivity area northeast of where Survey B started with an average resistivity value approximately 125Ωm. This could be the beginning of the Pinto Basin as the relationship between location B → C → D appears to be two distinct areas

separated by location C, or as mentioned, C is a divider between what would be a contiguous layer B→ D.

Location E, shows oscillations in resistivity that have a "U" shape stretching into the subsurface are uniformly spaced when present, correlating to electrode placement. These oscillations are likely the result of the application of a high salt content solution in vicinity of the electrode in order to improve contact resistance, as discussed above.

5.3 Comparisons and Findings

The shallow wet layer is shared between both surveys. Its path is directly attributed to being in a wash, and is likely the infiltrated overland flow from the 13 October 2018 precipitation event. Both washes in both surveys are also underlain by a higher resistivity layer although the resistivity of these layers between to the two surveys are different suggesting a change in the composition of the layer. The difference in resistivity is approximately 250Ωm. Since resistivity is not a precise measurement tool for substrate identification, the measured resistivities can indicate a range of possible materials. The relatively low resistivity suggests unconsolidated alluvial deposits which would remain consistent with the driller's logs and other interpreted geological characteristics. Furthermore, resistivity increases as the level of consolidation increases in unconsolidated materials.

The subsurface high resistivity layers that lie beneath the low resistivity layer in both surveys are quite different with respect to resistivity measurements. The resistivity values of the higher resistance area in Survey B are nearly 2.5x greater than the area in Survey A, and it also extends from depth closer to the surface. This trend is consistent with exposed bedrock in the local vicinity, as the uplifting or folding of bedrock could bring higher resistivity layers closer to the ground surface. The older the alluvial deposits become, the greater the resistivity

measurements tend to be as a result of deformation, compaction, and cementation. From geological interpretation we know the older alluvial deposits are closer to bedrock, and could suggest that these measured higher resistivity areas are on top of the bedrock. Since this measured area is only 109m at depth, the potential for bedrock to be below these materials is consistent with all available data. The exposed bedrock in vicinity of the study area in addition to the aforementioned interpretation of the high resistivity areas could indicate that a groundwater connection between the two basins is unlikely.

Both surveys show evidence of oscillations at electrode locations that provide good evidence of localized lowering of resistivity due to the introduction of a salt water solution to the natural environment. This observation is most apparent when the natural subsurface in vicinity of the electrode has a higher resistivity such as that in Survey A around 340m from the start of the survey.

5.4 Geochemical Discussion

This study compared the 2009 water quality analysis from the Mathany et al. (2012) and this analysis in 2018, presented in Table 4-1. No significant variation in major ion values were evident over the 9-year span between sampled measurements, suggesting that pumping has not pulled in water of varying compositions from other areas or any groundwater contamination events have occurred.

Regarding stable isotopes of water, δD (Deuterium) is measured at -71 ‰ relative to Vienna Standard Mean Oceanic Water (VSMOW) and $\delta^{18}O$ is -9.80 ‰ relative to VSMOW. These stable isotope values are nearly identical to the values sampled in 2009 (Mathany, 2012). The resulting comparison to the global meteoric water line (GMWL) ($\delta^{2}H = 8\delta^{18}O + 10‰$) shows that it shares a relatively comparable fractionation compared to the GMWL (Figure 5-1).

Surface or near surface evaporation causes water to become progressively enriched in these isotope values since the isotopes ^{2}H and ^{18}O are heavier and less susceptible to evaporation. In the event the sampled waters experience evaporative fractionation, they would become more isotopically enriched, which would plot to the right of and below the GMWL. Since the measurement shows little enrichment or deviation from the GMWL it does not appear that evaporation has had a significant effect on this recharge. JOTR maintains one of the lowest humidity averages in the country. For 2018, average annual humidity measurements range between 21-42% humidity (NOAA, 2018) in JOTR, being relatively low for the United States. Thus, recharge events to the aquifer likely occurred during cooler and wetter periods. This observation is consistent with the Pleistocene lacustrine deposits that are below the young alluvium but above the old alluvium in the subsurface according to Weir & Bader (1963). Precipitation collection and isotope analysis could help provide information on modern recharge.

5.5 Potential Routes of Groundwater Contamination

The results of geochemical analysis (Table 4-1) indicates there has not been any contamination to this groundwater. All parameter values measured are the same or very close as sampled 9 years ago, suggesting little variation from pumping of groundwater. The only known potential area for contamination is the leach fields from the Cottonwood visitor center septic system. Figure 5-2 shows both the current leach field and the proposed leach field locations. Proposed leach fields will be greater than 2x larger than the current leach field. The groundwater well is 4.27 km (2.66 miles) from the current leach fields and approximately the same distance for the proposed new leach fields. However, hydrogeologic conditions and current leach field installation practices will likely remove any contaminants well in advance of water being withdrawn that is tied to the leach field. One primary indication of septic system failure would be

increased nitrate levels in groundwater and between sampling in 2009 and 2018 nitrate levels remain consistent at 1.5 mg/L (Mathany et al., 2012). Lack of contamination indications or any illnesses has not prompted any investigation into fecal coliforms nor has this study investigated such. This does not mean other contaminates are not present in the LUB-23, such as emerging organic contaminants (EOC), and may be an area of interest to investigate in the future.

5.6 Well Observations Discussion

Observations during the well investigation do not suggest any clogging or circumstances that would interfere with the function of a screened well. Particulates become more evident with increasing depth, but not to a degree that should inhibit function. Although the investigation did not continue to the total depth of the well, nothing indicates poor performance.

Poor well performance was one of the potential rationales as to why the water level in vicinity of LUB-23 seemed to be dropping. In 2018 Park Service personnel reported a depth to water at LUB-23 of 67m (219 ft) bgs. This investigation found depth to water of 58m (191 ft) bgs, almost ~9m (30ft) difference. The difference between these two water levels cannot be explained within the limits and course of this research. Seasonal variations, an improper reading, or fluctuations of outflows and inflows could explain the large difference in water level readings. The original water level when LUB-23 was installed in 1958 was 52m (170ft) bgs. With the Cottonwood springs outflow and over 50 years of groundwater extraction, this 6m (20ft) decline is not unreasonable but presents evidence for concern for how future groundwater extraction from this small sub-basin is managed; small changes could result in a large impact.

The current measure of LUB-23 water level further substantiates the lack of a groundwater connection. The surface elevation is higher at LUB-23 (~900m above sea level asl) and lower near the fault zone (~890m asl) bordering the Pinto Basin. With the observed water

level at 52m (170ft) bgs and exposed bedrock near the fault zone, it is unlikely the basin could possibly fill to a point to spill over. The bedrock in this area is impermeable and there is no evidence that suggest cracks or fractures that could facilitate through flow.

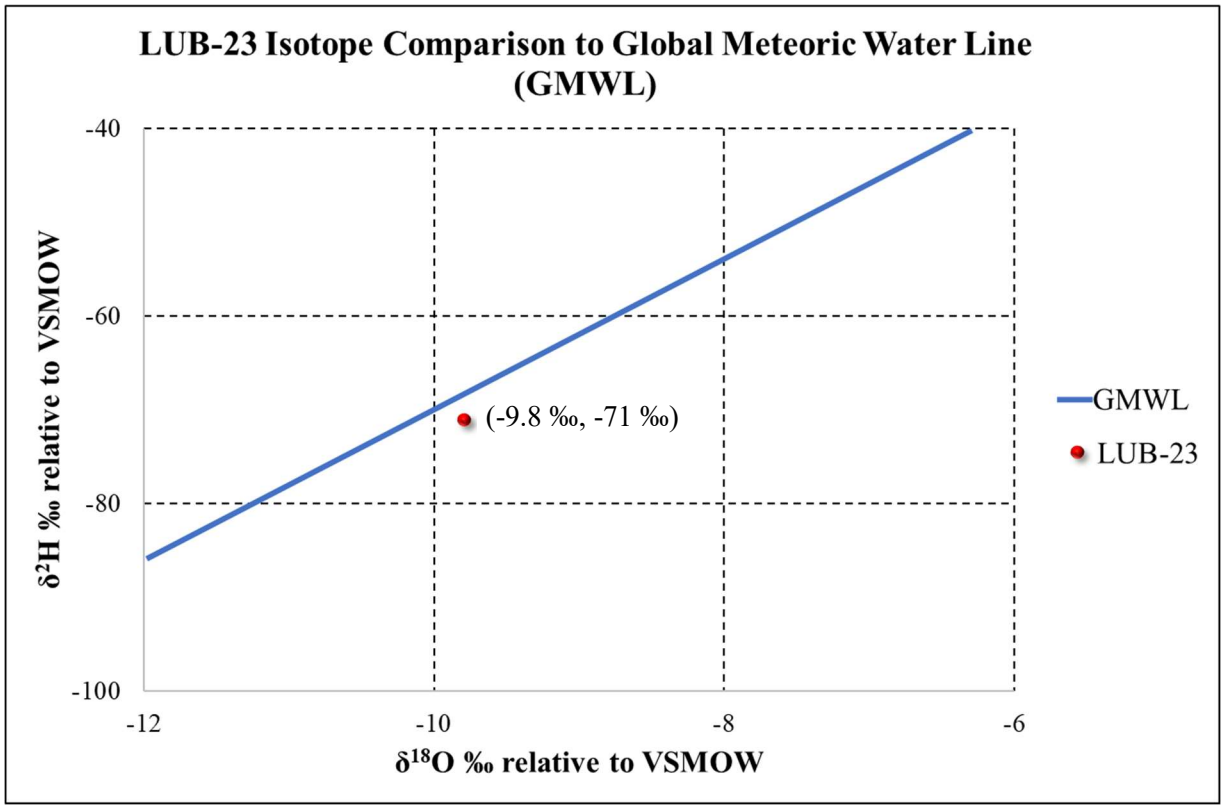

Figure 5-1. Global Meteoric Water Line (GMWL) comparison to LUB-23 measured stable isotopes of deuterium (^{2}H) and ^{18}O. GMWL source credit: Clark & Fritz, 1997.

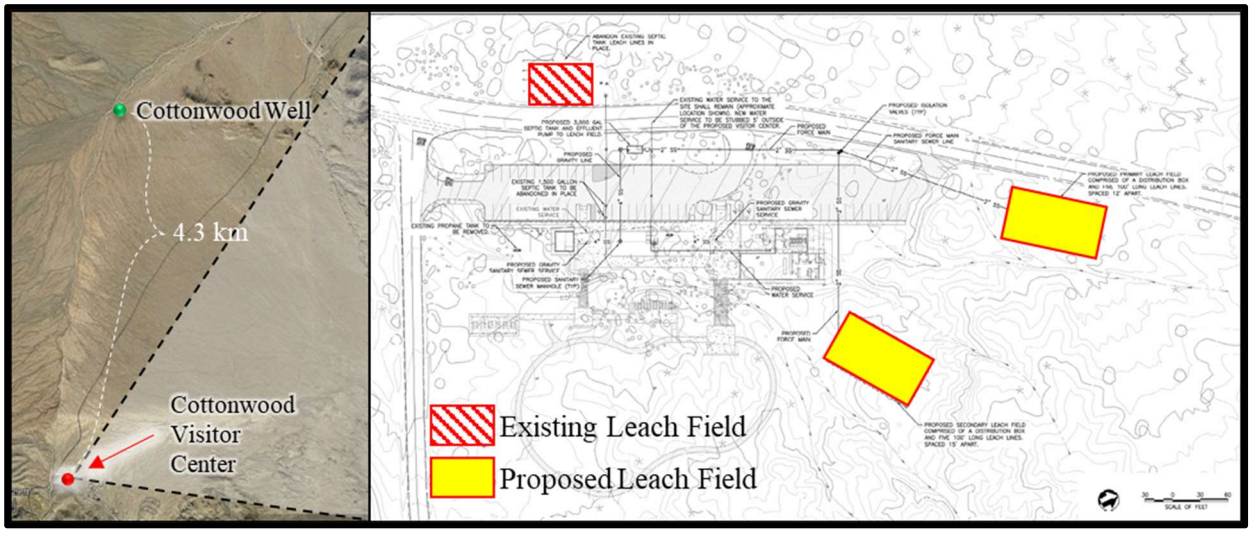

Figure 5-2. Existing and proposed leach fields for the septic system at the Cottonwood Visitor Center.

6. CONCLUSIONS

The purpose of this study was to investigate potential groundwater connections between the Cottonwood sub-basin and the Pinto Basin. The area chosen to conduct this investigation was an area determined by Karst & Rice (2018) as a potential fault zone, or most likely area for a connection to exist (Karst & Rice, 2018). If there was a groundwater connection between the Pinto Basin and the Cottonwood sub-basin via a fault-controlled spillway, we would expect to see two basic observations. First, evidence of a groundwater connection between the two basins and second, evidence of faulting. The conceptual scenarios of faulting conditions were referred to as Scenario A and Scenario B (Figure 1-5). However, the resulting resistivity contours do not show any evidence of a groundwater connection in the area where the survey was conducted. Additional corroborating evidence for a lack of a groundwater connection is the exposure of bedrock in the near vicinity of the surveys and water levels. The water table of the Cottonwood sub-basin is well below bedrock elevations and high resistivity areas near the fault zone investigated with ERT. With the shallow depth to high resistivity layers, the exposure of bedrock in the vicinity, lack of a groundwater connection, and lack of faulting identified, this study concludes there is not a groundwater connection as an outflow from the Cottonwood sub-basin to the Pinto Basin. Therefore, the investigation has determined without a groundwater connection or definitive evidence of faulting, a fault-controlled spillway does not currently exist between the Cottonwood sub-basin and the Pinto Basin.

The reported depth to water of the aquifer of 219 ft was one of the following: (1) an incorrect measurement (2) taken while the pump was active or (3) an accurate reading and the water table rose nearly 30ft. During the course of this research the water level was logged at

190ft bgs which is ~30ft closer to the surface than what was previously reported at 219ft bgs. When the pump and recovery test was conducted, it was logged that while the pump was operating the water level declined to a maximum depth of 198.68 ft bgs after the pump was operating for only 15 minutes. If the water level was taken while the pump was operating, it would not reflect an accurate static water table, as is intended.

Karst & Rice (2018) suggested a secondary location for an observation well or alternate well as labeled in Figure 3-4 (Karst & Rice, 2018). Existing seismic and gravity data in addition to the ERT results from this study reinforce the recommendation that the alternate well to be south of LUB-23 along the road in the deepest part of the Cottonwood sub-basin consistent with its approximate placement in Figure 3-4.

A proposed explanation by Karst & Rice (2018) regarding the decline in water table also noted that the well screen could be clogged, which reduces the efficiency of the well and may promote the appearance of a declining water table over time (Karst & Rice, 2018). Following a short pumping test as well as visually observing the well screening with a subsurface camera, there does not appear to be any degradation of efficiency in LUB-23 despite its 60-year age.

Geochemical and stable isotope analyses indicate that there has been little or no change since 2009, suggesting that the volume of water extracted from LUB-23 is minor compared to the volume of water in the aquifer and there are no contaminant concerns.

7. RECOMMENDATIONS

An understanding of the precipitation vs. infiltration in Cottonwood sub-basin would help refine a more accurate water budget. It appears, that when there is overland flow through the washes, a lot of potential recharge is lost to the Pinto Basin and could contribute to the outflow assumption in the water budget by Karst & Rice (2018). Understanding how much recharge is retained in the Cottonwood sub-basin from a precipitation event could help to develop an accurate water budget and gauge sustainable groundwater development. Current data may be misrepresentative of the specific area of interest regarding recharge potential, due to the lack of local gaging stations. A thorough understanding of the hydraulic gradient throughout the sub-basin would aid in determining ground water flow directions and rates.

Groundwater modeling could be of benefit to see how much of the shallow infiltration flows to the deeper parts of the Cottonwood sub-basin versus flowing out into the Pinto Basin. For example, the observed saturation layer from the recent precipitation event (Figure 4-9, Location A) shows evidence that saturated area above higher resistivity layer is not permanent. The water may travel out of the Cottonwood sub-basin since the local hydraulic gradient at shallow depths follows the topographic relief of the Cottonwood sub-basin to the Pinto Basin. To be able to quantify this would contribute to improving the development of a local water balance.

ERT collection utilizing longer arrays should be completed to better confirm the deepest areas of bedrock in addition to broadening the scope of ERT utilization into 3 dimensions. Executing a box technique may be able to provide a more comprehensive understanding of the subsurface in the fault zone to reinforce the findings of this research and specifically identify the presence of faults. A box technique in ERT utilizes multiple lines to create a 3-dimensional

model that includes length, width, and depth. This study utilized 2-dimensional analysis. Employing an ERT survey that can visualize down to the depth of bedrock in the Pinto Basin along the boundary of the Cottonwood sub-basin and the Pinto Basin would be substantially useful definitively proving the relationship between these two basins.

By suggesting that there is not a fault-controlled spillway between the Cottonwood sub-basin and the Pinto basin, we contribute to Karst and Rice's assumption that the Cottonwood sub-basin is isolated from underflows (both in and out) in not just the south and west, but in the area surveyed in this studies (northeast) (Karst & Rice, 2018).

On 13 October 2018, 2.33" of rain fell in the vicinity of the Cottonwood sub-basin which caused flash flooding and destroyed parts of the primary roadway and infrastructure in the southern part of the park. It would be of benefit to conduct future studies in the fluvial geomorphological sense and gauging the characteristics of runoff to better prepare, improve, or alleviate future vulnerabilities to flash flooding; similar to the study by Bastawesy et al (2019) in eastern Egypt.

A monitoring or secondary well in the location recommended by Karst & Rice (2018) would be beneficial to observe and confirm the drawdown data of this aquifer to determine transmissivity and specific yield. It could also be used as a contingency well in the event one well becomes inoperable, as this one well feeds the entirety of the southern park. A useful course of action would be to install a new well at the indicated location and turn LUB-23 into a monitoring well.

REFERENCES

Advanced Geosciences, Inc. (AGI) (2009). EarthImager 2D Resistivity and IP Inversion Software Instruction Manual. Copyright.

Advanced Geosciences, Inc (AGI) (2018). *How To Conduct An Electrical Resistivity Survey In 9 Easy Steps*. https://www.agiusa.com/how-conduct-electrical-resistivity-survey-9-easy-steps. Accessed 01 November 2018.

Aizebeokhai, & Oyeyemi. (2014). The use of the multiple-gradient array for geoelectrical resistivity and induced polarization imaging. Journal of Applied Geophysics, 111, 364-376.

Ammar, A., and K. Kamal, (2018). "Resistivity Method Contribution in Determining of Fault Zone and Hydro-geophysical Characteristics of Carbonate Aquifer, Eastern Desert, Egypt." Applied Water Science 8.1 (2018): 1-27. Web.

Asch, Ted; Abraham, Jared; & Irons, Trevor (2015). A Discussion on Depth of Investigation in Geophysics and AEM Inversion Results. *Conference Proceedings* XRI Geophysics, 15 August 2015.

Aydin, A., & Nur, A. (1982). Evolution of pull-apart basins and their scale independence. Tectonics, 1(1), 91-105.

Bastawesy, Attwa, Abdel Hafeez, and Gad (2019). "Flash Floods and Groundwater Evaluation for the Non-gauged Dryland Catchment Using Remote Sensing, GIS and DC Resistivity Data: A Case Study from the Eastern Desert of Egypt." *Journal of African Earth Sciences* 152 (2019): 245-55. Web.

Barker, R. (1989). Depth Of Investigation Of Collinear Symmetrical 4-Electrode Arrays. Geophysics, 54(8), 1031-1037.

Bedrosian, P. A., Burgess, M. K., & Nishikawa, T. (2013). Faulting and groundwater in a desert environment; constraining hydrogeology using time-domain electromagnetic data. Near Surface Geophysics, 11(5), 545–555. https://doi-org.ezproxy2.library.colostate.edu/10.3997/1873-0604.2013043

Bense, Gleeson, Loveless, Bour, and Scibek, (2013) "Fault Zone Hydrogeology." Earth-Science Reviews 127 (2013): 171-92. Web.

Binley, A. (2015). Tools and techniques: electrical methods. In: Schubert, G. (Ed.), 2nd ed. Treatise on Geophysics 11. Elsevier, Oxford, UK, pp. 233–259. https://doi.org/10.1016/B978-0-444-53802-4.00192-5.

Burger, Robert H., Sheehan, Anne F., Jones, Craig H. (2006) “Introduction to Applied Geophysics; Exploring the Shallow Subsurface. (Reprint, 1992) (CD-ROM Included).” Scitech Book News, vol. 30, no. 3, 2006.

Campbell, E. W. C., and Campbell, W. H., (1935). The Pinto basin site: Southwest Museum Papers no. 9 Highland Park, Calif., p. 21-51.

Clark, Ian D., and Fritz, Peter (1997). *Environmental Isotopes in Hydrogeology*, ISBN: 1566702496, CRC Press, New York.

Cubbage, B., Noonan, G., & Rucker, E. (2017). A Modified Wenner Array for Efficient Use of Eight-Channel Resistivity Meters. Pure and Applied Geophysics, 174(7), 2705-2718.

Edwards, L. (1977). A modified pseudosection for resistivity and IP. Geophysics, 42(5), 1020-1036.

Greenwood, Jason (AGI Employee). Personal Interview. 04 April 2019.

Harder, E.C., (1912) *Iron-ore deposits of the Eagle Mountains*, California: U.S. Geol. Survey Bulletin, 503, p.81.

Heynekamp, Michiel R., Laurel B. Goodwin, Peter S. Mozley, William C. Haneberg, and Moore, J. Casey, (1999) "Controls on Fault-zone Architecture in Poorly Lithified Sediments, Rio Grande Rift, New Mexico; Implications for Fault-zone Permeability and Fluid Flow." Geophysical Monograph 113 (1999): 27-49. Web.

Jenkins, O. P., (1938), Geologic map of California: California Div. Mines.

Karst, Gary & Rice, Steve (2018). Evaluation of Groundwater Withdrawal Impacts Associated with the Proposed Expansion of the Cottonwood Campground Visitor Center, Joshua Tree N.P, technical memorandum. United States Department of the Interior, National Park Service, Water Resources Division, Fort Collins, CO; April 23, 2018.

Kunkel, F., & United States National Park Service. (1963). Hydrologic and geologic reconnaissance of Pinto Basin, Joshua Tree National Monument, Riverside County, California (Hydrology of the public domain). Washington, D.C.: U.S. G.P.O.

Langenheim, V., & Geological Survey issuing body. (2016). High-resolution gravity and seismic-refraction surveys of the Smoke Tree Wash area, Joshua Tree National Park, California (U.S. Geological Survey open-file report; 2016-1027). Reston, Virginia: U.S. Department of the Interior, U.S. Geological Survey.

Lewis, R., Geological Survey, Water Resources Division, & Mojave Water Agency. (1972). Ground-water resources of the Yucca Valley-Joshua Tree area, San Bernardino County, California (Open-file report (Geological Survey (U.S.)). Menlo Park, Calif.: U.S. Dept. of the Interior, Geological Survey, Water Resources Division.

Mathany, T., Michael T. Wright, Brandon S. Beuttel, and Kenneth Belitz Ground Water Ambient Monitoring Assessment Program, California. State Water Resources Control Board, & Geological Survey. (2012). Groundwater-quality data in the Borrego Valley, Central Desert, and low-use basins of the Mojave and Sonoran Desert study unit, 2008-2010 results from the California GAMA Program (Data series (Geological Survey; 659). Reston, Va.: U.S. Dept. of the Interior, U.S. Geological Survey.

Mcclay, K., & Dooley, T. (1995). Analog models of pull-apart basins. Geology, 23(8), 711-714.

Mclachlan, Chambers, Uhlemann, & Binley. (2017). Geophysical characterization of the groundwater–surface water interface. Advances in Water Resources, 109, 302-319.

Mendenhall, W.C. (1909). *Some desert watering places in southeastern California and southwestern Nevada*: U.S. Geological Survey Water-Supply Paper 224, p.98.

Miller, W. J., (1938) Pre-Cambrian and associated rocks near Twentynine Palms, California: Geol. Soc. America Bull., v.49, no. 3, p. 417-446.

Mohamaden, M.I.I., H.M. El-Sayed, and S.A. Mansour, (2017). "Combined Application of Electrical Resistivity and GIS for Groundwater Exploration and Subsurface Mapping at Northeast Qattara Depression, Western Desert, Egypt." Egyptian Journal of Basic and Applied Sciences 4.1 (2017): 80-88.

Monahan, Sara Michelle (2013), "Investigating Fault Structure Using Electrical Resistivity Tomography" Thesis Fulfillment, California Polytechnic University, November 2013.

Naranjo, Gema, Tatiana Cruz-Fuentes, and Emilio Custodio. "Estimating Natural Recharge by Means of Chloride Mass Balance in a Volcanic Aquifer: Northeastern Gran Canaria (Canary Islands, Spain)." *Water* 7.6 (2015): 2555-574. Web.

National Oceanic and Atmospheric Administration (NOAA) (2018). Record of Climatological Observations: Station: JOSHUA TREE 2.0 S, CA US US1CASR0014, Elev: 3409 ft Lat: 34.0973° N Lon: -116.3178° W, Generated 2/14/2019, https://www.nws.noaa.gov/

Nishikawa, Izbicki, Hevesi, Stamos, Martin, & Nishikawa, T. (2004). Evaluation of Geohydrologic Framework, Recharge Estimates, and Ground-Water Flow of the Joshua Tree Area, San Bernardino County, California, 132.

Oldenburg, D., & Li, Y. (1999). Estimating depth of investigation in DC resistivity and IP surveys. Geophysics, 64(2), 403-416.

Ozsvath, David. "Fluoride Concentrations in a Crystalline Bedrock Aquifer Marathon County, Wisconsin." *Environmental Geology* 50.1 (2006): 132-38. Web.

Ojo, Xie, & Olorunfemi. (2018). Nonlinear inversion of resistivity sounding data for 1-D earth models using the Neighbourhood Algorithm. Journal of African Earth Sciences, 137, 179-192.

Powell, R.E., 2001, Geologic map and digital database of the Porcupine Wash 7.5 minute quadrangle, Riverside county, California: U.S. Geological Survey Open-File Report 01–030, accessed November 15, 2005, at http://pubs.usgs.gov/of/2001/0030/

Powell, R.E., Matti, J.C., Cossette, P.M., 2015, Geology of the Joshua Tree National Park geodatabase: U.S. Geological Survey Open-File Report 2015–1175, GIS database, http://dx.doi.org/10.3133/ofr20151175.

Reynolds, J. (1997). An introduction to applied and environmental geophysics. Chichester ; New York: John Wiley.

Sada, D. W., and Jacobs, C. A., 2008, Environmental and biological characteristics of springs in Joshua Tree National Park, California, Great Basin Cooperative Ecosystem Studies Unit Task Agreement No. J8R07050014, 59 p.

Scanlon, B.R., Healy, R.W., and Cook, P.G., 2002, Choosing appropriate techniques for quantifying groundwater recharge: Hydrogeology Journal, v. 10, p. 18-39

Scharf, David (1935). The Quarternary history of Pinto basin: Southwest Museum Papers no. 9. Highland Park, Calif., p. 11-20.

Sibson, Richard H. (1981). "Controls on Low-stress Hydro-fracture Dilatancy in Thrust, Wrench and Normal Fault Terrains." Nature 289.5799 (1981): 665-667. Web.

Sibson, R. H., J. M. Moore, and A. H. Rankin, (1975). "Seismic Pumping; a Hydrothermal Fluid Transport Mechanism." Journal of the Geological Society of London 131.6 (1975): 653-59. Web.
Stummer, P., Maurer, H., and Green, A.G. (2004). Experimental design: Electrical resistivity data sets that provide optimum subsurface information, Geophysics, vol 69, 120-139.

"Supersting™ - WiFi" *Advanced Geosciences Inc. (AGI),* 10 April 2019, https://www.agiusa.com/supersting-wifi.

Trent, D.D. & Hazlett, Richard W., (2002) *Joshua Tree National Park Geology,* Twentynine Palms, CA, Joshua Tree National Park Association, ISBN: 0-9679756-1-1, 2002.

United States Geological Survey (USGS), (2019), *Earthquake Hazard Program*: https://earthquake.usgs.gov/ Accessed 03 May 2019.

Weir Jr., J.E., Bader, J.S., & United States National Park Service & Geological Survey issuing body (1963). Ground water and related geology of Joshua Tree National Monument, California (U.S. Geological Survey open-file report: 63-137). Long Beach, California: U.S. Department of the Interior, U.S. Geological Survey

Winters, Ryvkin, Rudkov, Moreno, and Furman (2015) "Mapping Underground Layers in the Super Arid Gidron Wadi Using Electrical Resistivity Tomography (ERT)." *Journal of Arid Environments* 121 (2015): 79-83.

APPENDIX 1. CONTACT RESISTANCE MEASUREMENTS

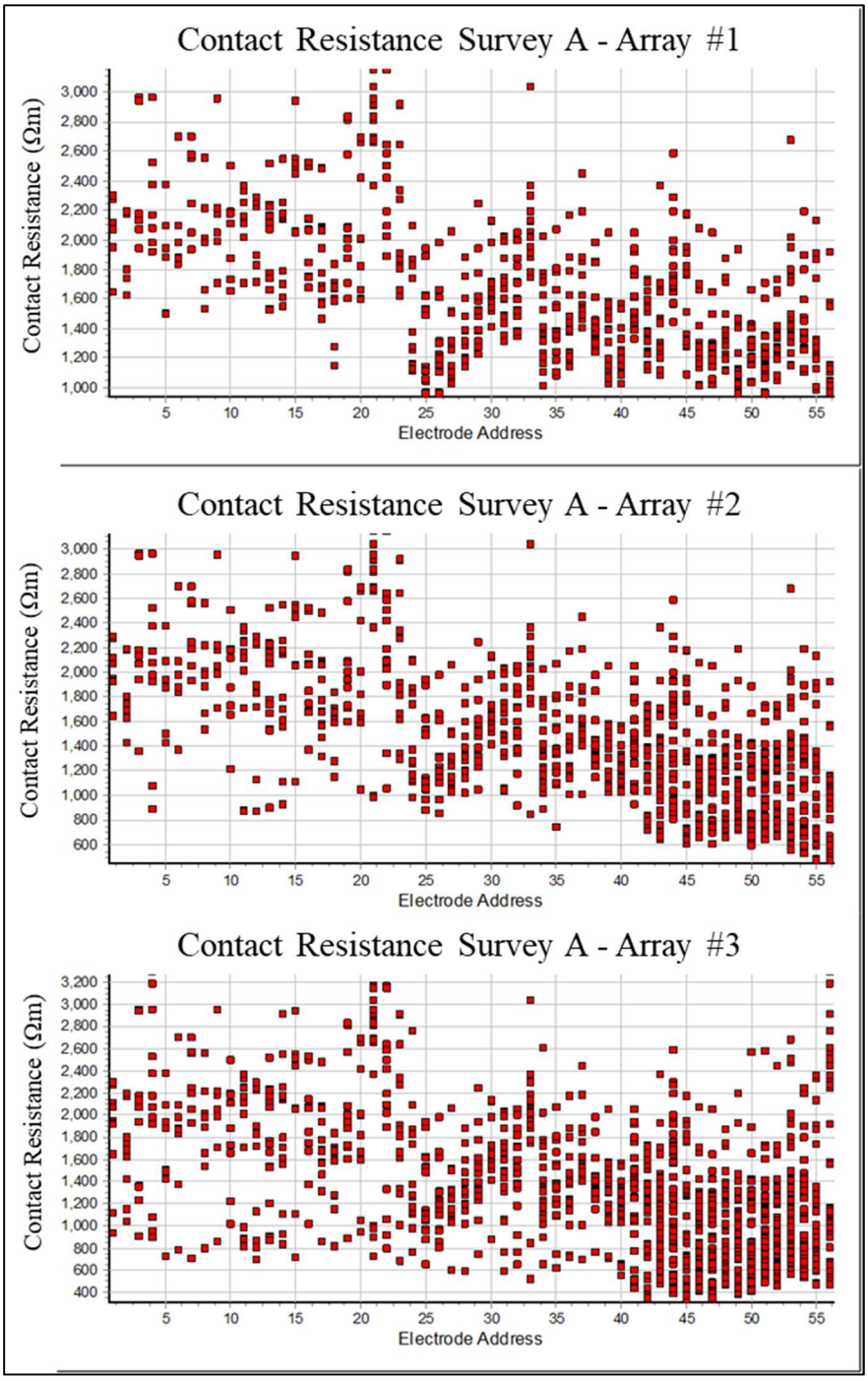

Figure 7-1. Contact resistance for each electrode for each array run for Survey A.

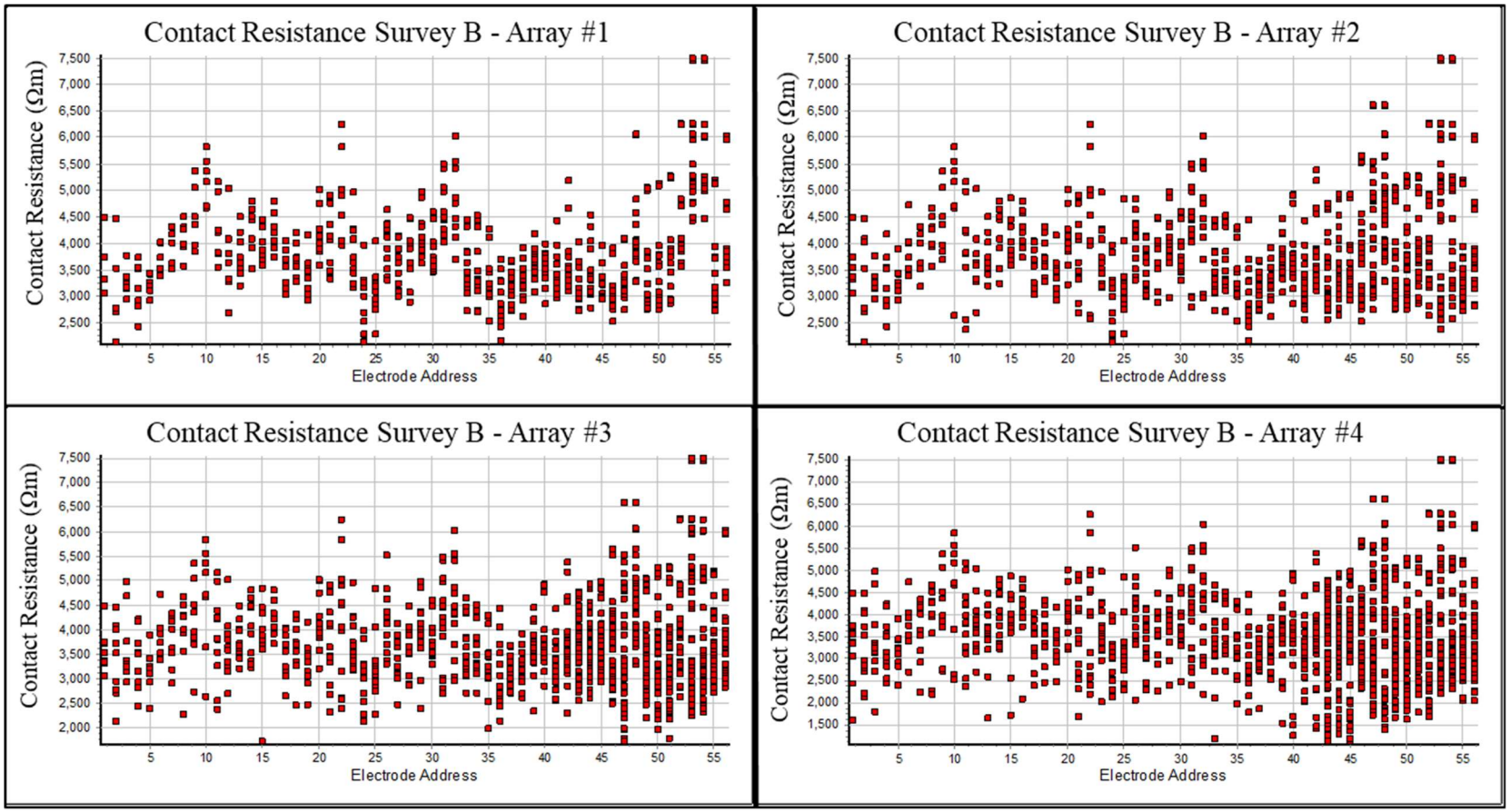

Figure 7-2. Contact resistance for each electrode for each array run for Survey B.

APPENDIX 2. FIELD DATA COLLECTION LOCATIONS

Table 8-1. UTM locations for locations referenced in study

Location Description	UTM Zone	UTM Easting	UTM Northing
Cottonwood Well (LUB-23)	11S	0609628	3739114
Cottonwood Visitor Center	11S	0608920	3734895
Leaking Spigot	11S	0609598	3739136
Generator House	11S	0609612	3739145
Solar Panel Farm	11S	0609627	3739137
Cottonwood Springs	11S	0610255	3733598
Well Storage Tank	11S	0609254	3734090
UTM: Universal Transverse Mercator coordinate system			

Table 8-2. UTM locations for electrode land cable points for Survey A

ERT Survey A Locations					
Point ID	**Point Description**	**UTM Zone**	**UTM Easting**	**UTM Northing**	**Elevation(m)**
0001	Start Point	11S	0609740	3739356	891
0002	Start of 2nd line	11S	0609663	3739232	899
0003	Start of 3rd line	11S	0609602	3739099	907
0004	Start of 4th line	11S	0609559	3738959	911
0005	Start of 5th line	11S	0609512	3738822	915
0006	Start of 6th line	11S	0609472	3738689	917
0007	End Point	11S	0609425	3738552	919

Table 8-3. UTM locations for electrode land cable points for Survey B

ERT Survey B Locations					
Point ID	**Point Description**	**UTM Zone**	**UTM Easting**	**UTM Northing**	**Elevation(m)**
0008	Start Point	11S	0610691	3740104	889
0009	Start of 2nd line	11S	0610834	3740137	887
0010	Start of 3rd line	11S	0610977	3740155	887
0011	Start of 4th line	11S	0611120	3740186	885
0012	Start of 5th line	11S	0611255	9740235	884
0013	Start of 6th line	11S	0611388	3740305	882
0014	Start of 7th line	11S	0611526	3740338	881
0015	End Point	11S	0611659	3740345	881

APPENDIX 3. DATA COLLECTION PHOTOS

Figure 9-1. Photo of the Generator House. Tyler Gilkerson (left) and John Boyle (right); prior to setup 11/26/18.

Figure 9-2. John Boyle installing an electrode into the ground for Survey A, along the road. 11/26/18.

Figure 9-3. John Boyle (background), Mary (center), and Tyler Gilkerson (right) unraveling electrode land cable lines setting up Survey A. 11/26/18.

Figure 9-4. John Boyle setting up the AGI Supersting^{TM} at the center point of Array 1 of Survey A along the road. 11/26/18.

Figure 9-5. Steven Rice (left) and John Boyle (right) recording contact resistance measurements for Survey A. 11/26/18.

Figure 9-6. John Boyle utilizing the 5-Gallon backpack sprayer with salt-water solution to saturate electrodes in order to improve contact resistance. 11/26/18.

Figure 9-7. Dr. William Sanford (top center), John Boyle (top right), and Steven Rice (right) reviewing initial inversion resistivity for Array 1, Survey A. 11/26/18.

Figure 9-8. Dr. Sanford (left), Tyler Gilkerson (center-right), and Steven Rice (right) hauling equipment into the Wilderness for Survey B. The most difficult and time-consuming part of this study. 11/27/18.

Figure 9-9. Tyler Gilkerson using the 5-gallon backpack sprayer to saturate the electrodes to help improve contact resistance for Survey B.

Figure 9-10. John Boyle (background left), Dr. William Sanford (background right), Steven Rice (center) and Luke Sabala (JOTR Science Div) (left), inspect lines and run initial contact resistance tests for Survey B. 11/27/18.

Figure 9-11. A length of Survey B in the wash after applying the salt water solution to the electrodes in order to improve contact resistance. 11/27/18.

Figure 9-12. John Boyle (left), Dr. William Sanford (left-center), Steven Rice (right-center), and Luke Sabala (right) discussing the meaning of the initial inversion results for Survey B. 11/27/18.

Figure 9-13. Steven Rice (left), John Boyle (left-center), Dr. William Sanford (right-center), and Allison Dunkel (right) setting up the digital camera to inspect inside LUB-23. 11/28/18

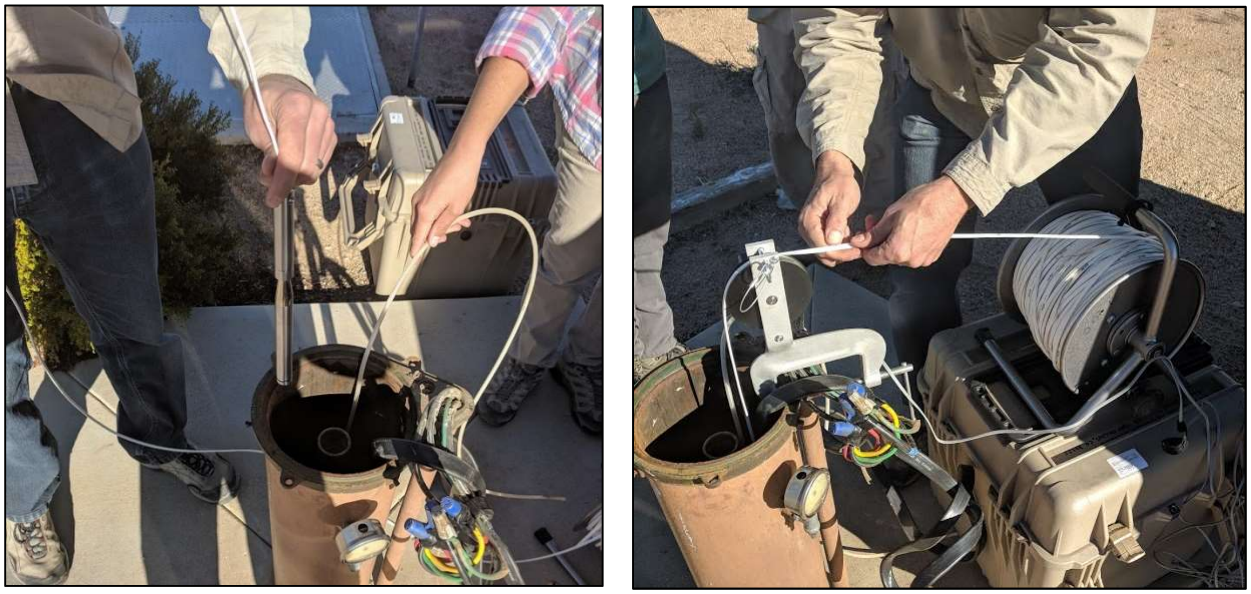

Figure 9-14. Steven Rice and Allison Dunkel lowering the digital camera into LUB-23. 11/28/18.

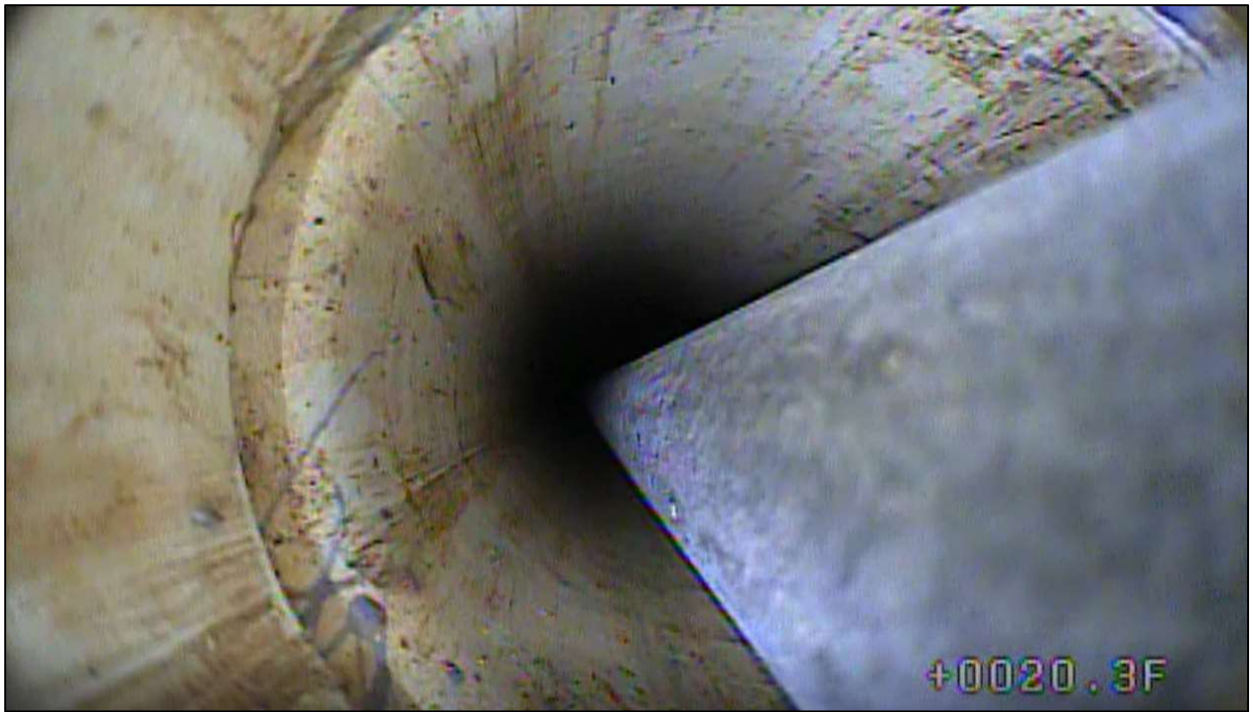

Figure 9-15. Camera screenshot inside LUB-23 at a spool length of 20.3 ft, and 17.9 ft below ground surface (the well entry point is 2.4 ft above ground surface). 11/28/18.

Figure 9-16. Camera screenshot inside LUB-23 at a spool length of 192.8 ft. Notice the water level just below the camera. The precise reading at that water level is 193.18 ft from spool or 190.78 ft bgs.

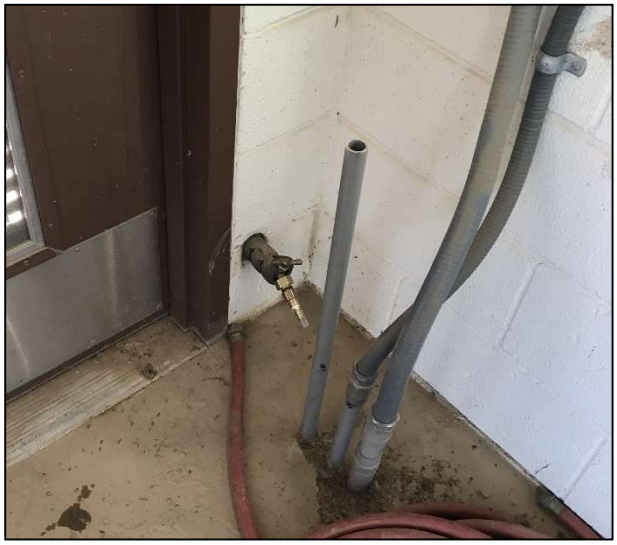

Figure 9-17. A spigot inside the generator house that is connected to LUB-23 well water (pre-treatment). This is the source for water sampled for geochemical analysis.

Figure 9-18. Photo of the solar panel farm.

Figure 9-19. John Boyle (left) and Dr. William Sanford (right) using Hach Method 8203 to determine alkalinity of LUB-23 well water. 11/28/18.

Figure 9-20. John Boyle using the Oakton multi-parameter PC Testr-35 to measure pH, conductance, water temperature, and dissolved oxygen of LUB-23 well water. 11/28/18.

Figure 9-21. The leaking spigot near the generator house, a continual small pool of water is present year-round.

APPENDIX 4: Test America Methods & Results

TestAmerica

THE LEADER IN ENVIRONMENTAL TESTING

ANALYTICAL REPORT

TestAmerica Laboratories, Inc.
TestAmerica Irvine
17461 Derian Ave
Suite 100
Irvine, CA 92614-5817
Tel: (949)261-1022

TestAmerica Job ID: 440-225417-1
Client Project/Site: Joshua Tree - Cottonwood

For:
National Park Service
Aquatic Systems
1201 Oakridge Dr
Ste 250
Fort Collins, Colorado 80525

Attn: Steve Rice

Authorized for release by:
1/7/2019 9:13:21 AM

Janice Hsu, Project Manager I
(949)261-1022
janice.hsu@testamericainc.com

LINKS

Review your project results through TotalAccess

Have a Question? Ask The Expert

Visit us at: www.testamericainc.com

The test results in this report meet all 2003 NELAC and 2009 TNI requirements for accredited parameters, exceptions are noted in this report. This report may not be reproduced except in full, and with written approval from the laboratory. For questions please contact the Project Manager at the e-mail address or telephone number listed on this page.

This report has been electronically signed and authorized by the signatory. Electronic signature is intended to be the legally binding equivalent of a traditionally handwritten signature.

Results relate only to the items tested and the sample(s) as received by the laboratory.

Case Narrative

Client: National Park Service
Project/Site: Joshua Tree - Cottonwood

TestAmerica Job ID: 440-225417-1

Job ID: 440-225417-1

Laboratory: TestAmerica Irvine

Narrative

Job Narrative
440-225417-1

Comments
No additional comments.

Receipt
The sample was received on 11/29/2018 12:00 PM; the sample arrived in good condition, properly preserved and, where required, on ice. The temperature of the cooler at receipt was 5.8º C.

HPLC/IC
Method(s) 300.0: The matrix spike / matrix spike duplicate (MS/MSD) recoveries for the following sample associated with analytical batch 440-513892 were outside control limits: (440-225343-D-2 MS) and (440-225343-D-2 MSD). The associated laboratory control sample (LCS) recovery met acceptance criteria.

No additional analytical or quality issues were noted, other than those described above or in the Definitions/Glossary page.

RAD
Method(s) SM 7500-Rn B: Radon-222 Prep Batch 160-404021

The following samples were counted after four days from the sampled date. Analysis outside of this time period may result in a low bias to the measured results from the potential loss of radon due to its volatile nature. The laboratory believes this will be minimal for samples collected in the field according to method sampling instructions, Due to the relatively short half-life (3.82 days), delay in analysis will lead to an increase in the relative uncertainty reported with the measurement.

Smoke Tree Well (440-225417-1) and (440-225417-B-1-B DU)

No additional analytical or quality issues were noted, other than those described above or in the Definitions/Glossary page.

Metals
No analytical or quality issues were noted, other than those described in the Definitions/Glossary page.

General Chemistry
No analytical or quality issues were noted, other than those described in the Definitions/Glossary page.

Subcontract non-Sister
No analytical or quality issues were noted, other than those described in the Definitions/Glossary page.

Client Sample Results

Client: National Park Service
Project/Site: Joshua Tree - Cottonwood

TestAmerica Job ID: 440-225417-1

Client Sample ID: Smoke Tree Well

Lab Sample ID: 440-225417-1
Matrix: Water
Date Collected: 11/28/18 10:30
Date Received: 11/29/18 12:00

Method: 300.0 - Anions, Ion Chromatography

Analyte	Result	Qualifier	RL	MDL	Unit	D	Prepared	Analyzed	Dil Fac
Chloride	38		2.5	1.3	mg/L			11/29/18 22:10	5
Nitrate as N	1.5		0.11	0.055	mg/L			11/29/18 21:56	1
Fluoride	2.8		0.50	0.25	mg/L			11/29/18 21:56	1
Nitrite as N	ND		0.15	0.025	mg/L			11/29/18 21:56	1
Sulfate	27		0.50	0.25	mg/L			11/29/18 21:56	1

Method: 314.0 - Perchlorate (IC)

Analyte	Result	Qualifier	RL	MDL	Unit	D	Prepared	Analyzed	Dil Fac
Perchlorate	ND		4.0	0.95	ug/L			12/03/18 18:43	1

Method: 200.7 Rev 4.4 - Metals (ICP) - Total Recoverable

Analyte	Result	Qualifier	RL	MDL	Unit	D	Prepared	Analyzed	Dil Fac
Boron	0.13		0.050	0.025	mg/L		12/10/18 09:32	12/10/18 16:01	1
Calcium	34		0.10	0.050	mg/L		12/10/18 09:32	12/10/18 16:01	1
Iron	ND		0.10	0.050	mg/L		12/10/18 09:32	12/10/18 16:01	1
Magnesium	6.7		0.020	0.010	mg/L		12/10/18 09:32	12/10/18 16:01	1
Potassium	1.7		0.50	0.25	mg/L		12/10/18 09:32	12/10/18 16:01	1
Sodium	37		0.50	0.26	mg/L		12/10/18 09:32	12/10/18 16:01	1

Method: 200.8 - Metals (ICP/MS) - Total Recoverable

Analyte	Result	Qualifier	RL	MDL	Unit	D	Prepared	Analyzed	Dil Fac
Aluminum	9.5	J	10	5.0	ug/L		12/07/18 08:17	12/07/18 17:41	1
Antimony	ND		2.0	0.50	ug/L		12/07/18 08:17	12/07/18 17:41	1
Arsenic	2.2		1.0	0.50	ug/L		12/07/18 08:17	12/07/18 17:41	1
Barium	36		1.0	0.50	ug/L		12/07/18 08:17	12/07/18 17:41	1
Beryllium	ND		0.50	0.25	ug/L		12/07/18 08:17	12/07/18 17:41	1
Cadmium	ND		1.0	0.25	ug/L		12/07/18 08:17	12/07/18 17:41	1
Chromium	ND		2.0	0.50	ug/L		12/07/18 08:17	12/07/18 17:41	1
Copper	1.1	J	2.0	0.50	ug/L		12/07/18 08:17	12/07/18 17:41	1
Lead	ND		1.0	0.50	ug/L		12/07/18 08:17	12/07/18 17:41	1
Manganese	0.83	J	1.0	0.50	ug/L		12/07/18 08:17	12/07/18 17:41	1
Nickel	ND		2.0	0.50	ug/L		12/07/18 08:17	12/07/18 17:41	1
Selenium	1.6	J	2.0	0.50	ug/L		12/07/18 08:17	12/07/18 17:41	1
Thallium	ND		1.0	0.50	ug/L		12/07/18 08:17	12/07/18 17:41	1
Uranium	3.0		1.0	0.50	ug/L		12/07/18 08:17	12/07/18 17:41	1
Zinc	63		20	2.5	ug/L		12/07/18 08:17	12/07/18 17:41	1

General Chemistry

Analyte	Result	Qualifier	RL	MDL	Unit	D	Prepared	Analyzed	Dil Fac
Total Dissolved Solids	270		10	5.0	mg/L			12/01/18 10:11	1

Analyte	Result	Qualifier	RL	RL	Unit	D	Prepared	Analyzed	Dil Fac
Alkalinity as CaCO3	120		4.0	4.0	mg/L			11/30/18 04:31	1
Bicarbonate Alkalinity as CaCO3	120		4.0	4.0	mg/L			11/30/18 04:31	1
Carbonate Alkalinity as CaCO3	ND		4.0	4.0	mg/L			11/30/18 04:31	1
Hydroxide Alkalinity as CaCO3	ND		4.0	4.0	mg/L			11/30/18 04:31	1

Client Sample Results

Client: National Park Service
Project/Site: Joshua Tree - Cottonwood

TestAmerica Job ID: 440-225417-1

Client Sample ID: Smoke Tree Well
Date Collected: 11/28/18 10:30
Date Received: 11/29/18 12:00

Lab Sample ID: 440-225417-1
Matrix: Water

Method: C-01-1 - Carbon-14 (EERF C-01-1)

Analyte	Result	Qualifier	Count Uncert. (2σ+/-)	Total Uncert. (2σ+/-)	RL	MDC	Unit	Prepared	Analyzed	Dil Fac
Carbon-14	-4.03	U	7.02	7.03	20.0	12.1	pCi/L	12/23/18 08:28	12/24/18 16:19	1

Method: SM 7500-Rn B - Radon-222 (LSC)

Analyte	Result	Qualifier	Count Uncert. (2σ+/-)	Total Uncert. (2σ+/-)	RL	MDC	Unit	Prepared	Analyzed	Dil Fac
Radon 222	392		27.2	41.5	30.0	15.0	pCi/L	12/04/18 14:34	12/04/18 19:56	1

Method Summary

Client: National Park Service
Project/Site: Joshua Tree - Cottonwood

TestAmerica Job ID: 440-225417-1

Method	Method Description	Protocol	Laboratory
300.0	Anions, Ion Chromatography	MCAWW	TAL IRV
314.0	Perchlorate (IC)	EPA	TAL IRV
200.7 Rev 4.4	Metals (ICP)	EPA	TAL IRV
200.8	Metals (ICP/MS)	EPA	TAL IRV
SM 2320B	Alkalinity	SM	TAL IRV
SM 2540C	Solids, Total Dissolved (TDS)	SM	TAL IRV
C-01-1	Carbon-14 (EERF C-01-1)	EERF	TAL SL
SM 7500-Rn B	Radon-222 (LSC)	TAL-STL	TAL SL
200.2	Preparation, Total Recoverable Metals	EPA	TAL IRV
LSC_Dist_Susp	Distillation and Suspension (LSC)	None	TAL SL
NONE	Direct Addition Preparation for LSC	None	TAL SL

Protocol References:

EERF = EERF
EPA = US Environmental Protection Agency
MCAWW = "Methods For Chemical Analysis Of Water And Wastes", EPA-600/4-79-020, March 1983 And Subsequent Revisions.
None = None
SM = "Standard Methods For The Examination Of Water And Wastewater"
TAL-STL = TestAmerica Laboratories, St. Louis, Facility Standard Operating Procedure.

Laboratory References:

TAL IRV = TestAmerica Irvine, 17461 Derian Ave, Suite 100, Irvine, CA 92614-5817, TEL (949)261-1022
TAL SL = TestAmerica St. Louis, 13715 Rider Trail North, Earth City, MO 63045, TEL (314)298-8566